# Rate-Fairness-Aware Low Resolution RIS-Aided Multi-User OFDM Beamforming

H. Yu[1,2], H. D. Tuan[2], A. A. Nasir[3], E. Dutkiewicz[2], and L. Hanzo[4]

***Abstract*—This paper investigates reconfigurable intelligent surface (RIS)-aided OFDM network, where a multiple-antenna aided base station (BS) transmits its downlink (DL) signals to multiple single-antenna users via an RIS, which consists of a considerable amount of low-resolution programmable reflecting elements (PREs). Explicitly, we propose the joint design of the multi-user (MU) beamformers and the RIS's PREs for quality-of-service target in terms of the individual users' rates. In the face of dispersive channels, we demonstrate that this poses a large-scale mixed discrete continuous optimization problem of intractable nature. We then tackle this challenge by developing low-complexity iterative procedures, which invoke light-weight closed-form expressions at each iteration, are developed for its computational solution. The simulations demonstrate their computational efficiency and additionally, reveal the deficiencies of the conventional MU OFDM beamforming design based on sum-rate maximization.**

***Index Terms*—Reconfigurable intelligent surface, low bit-quantization, multi-user OFDM, quality-of-service, multi-objective beamforming, mixed discrete continuous optimization.**

## I. Introduction

Reconfigurable intelligent surfaces (RISs) are planar arrays of large number of programmable reflecting elements (PREs) and have emerged as an attractive wireless enabling technology [1], [2]. RIS-aided signal processing has recently received considerable research interest [3], [4]. However, the joint design of the PREs and multi-user (MU) beamformers has predominantly been limited to narrow-band scenario, when maximizing the users' sum rate (SR) [5]–[7] or their worst rate (WR) [8]–[10]. As a beneficial optimization objective function (OF), the geometric mean of the users' rates (GM-rate) has also been applied [11], [12] with the specific motivation of improving the fairness of users' rate. When maximizing the WR, the iterative optimization in [9] is based on convex problems of moderate dimension, which generate a sequence of gradually improved feasible points. By contrast, the iterations of [8], [10] are based on semi-definite relaxation (SDR) of excessive dimensions, which still cannot even finding a feasible point. For wide-band scenarios, the authors of [13]–[16] considered RIS-aided orthogonal frequency division multiple access (OFDMA) systems having base station (BS) equipped with a single-antenna, which assigns orthogonal bands for the single-antenna users. But again, all these solutions are based on iterating large-dimensional convex problems even for small-sized cases and thus having limited practical applications. For instance, the authors of [13] simulated a scenario of three users, 16 bands, and 80 PREs, while the authors of [14] simulated a scenario of two users, 32 bands, and 20 PREs.

OFDM is indeed the most popular protocol for combating frequency-selective multi-path propagation [17], hence a RIS-aided single-user single-input single-output (SISO) OFDM systems has been considered in [18]–[20]. All these treatises, along with [13]–[16] on OFDMA assumed the presence of direct paths from the BS to users, but for this scenario RISs hardly improve the system performance [9], [11], [12], [21].

While single-user OFDM is well documented [22], there are still open puzzles in MU OFDM in terms of managing the MU interference over each frequency band. As such, even the problem of power allocation maximizing the SR for SISO systems poses a large scale nonconvex optimization problem [23], [24]. Our recent work [25] is the first paper, which provides a computationally tractable solution for MU OFDM beamforming to maximize the SR of multiple input single output (MISO) systems. Furthermore, all the existing treatises on MU OFDM aim for optimizing the system's sum-rate. Our preliminary analysis in [25, Figs. 5 & 6] shows that maximizing the SR leads to zero rates for some users, i.e. their rates over all frequency bands are zero. This means that SR maximization leads to disconnect of some users and thus it is unsuitable for maintaining fairness in MU communications. The joint design of MU beamforming and RIS PREs for RIS-aided MU OFDM to maximize the SR of MISO systems has been documented in [26], which proposed to optimize one-by-one all the PRE with all other PREs held fixed for handling their constant modulus constraints.

Against the above background on RIS-less or RIS-aided OFDM communications, this paper is the first contribution, which aims for optimizing the rates of all users for the sake of meeting their quality-of-service (QoS) target. Regarding RISs, it also desirable that PREs having a low number of quantization bit for their practical implementation [27], [28].

[1]School of Communication and Information Engineering, Shanghai University, Shanghai, China (email: hw_yu@shu.edu.cn); [2] School of Electrical and Data Engineering, University of Technology Sydney, Broadway, NSW 2007, Australia (email: hongwen.yu@alumni.uts.edu.au, tuan.hoang@uts.edu.au, eryk.dutkiewicz@uts.edu.au); [3]Department of Electrical Engineering and Center for Communication Systems and Sensing King Fahd University of Petroleum and Minerals (KFUPM), Dhahran, Saudi Arabia (email: anasir@kfupm.edu.sa); [4]School of Electronics and Computer Science, University of Southampton, Southampton, SO17 1BJ, U.K. (e-mail: lh@ecs.soton.ac.uk).

H. Yu would like to acknowledge the financial support of Shanghai Sailing Scholar under Grant 23YF1412700; H. D. Tuan would like to acknowledge the financial support of Australian Research Councils Discovery Projects under Grant DP190102501; A. A. Nasir would like to acknowledge the financial support of Deanship of Research Oversight and Coordination (DROC) at KFUPM for funding under the Interdisciplinary Research Center for Communication Systems and Sensing through project No. INCS2203; L. Hanzo would like to acknowledge the financial support of the Engineering and Physical Sciences Research Council projects EP/W016605/1, EP/X01228X/1 and EP/Y026721/1 as well as of the European Research Council's Advanced Fellow Grant QuantCom (Grant No. 789028)

As such, a large-scale mixed discrete-continuous optimization problem is constituted by the joint design of PREs and beamforming, whose computational solution is unknown. Against this backdrop, the paper's contributions are three-fold:

- For solving the problem of maximizing the users' WR, an algorithm is developed, which iterates the convex problems for generating gradually improved PREs and MU beamformers;
- For solving the problem of maximizing the GM-rate, we develop an algorithm, which iterates closed-form expression for gradually enhancing both the PREs and MU beamformers for arbitrarily large networks. The iteration leads to a Pareto-optimal solution that achieves both high SR and high MR without an explicit QoS constraint involved, and the simulation results verified the advantages of our proposed GM rate optimization methods compared to the proposed SR and WR methods. This algorithm is also capable of solving the SR maximizing problem;
- Our simulations reveal that the conventional SR OF is unsuitable for MU OFDM as it leads to assigning zero rates to some users. By contrast, GM-rate optimization is capable of avoiding this deficiency while providing a good sum rate. As such GM-rate offers a Pareto optimized solution to the multi-objective SR and WR .

In summary, we boldly and explicitly contrast our novel contributions to the literature in Table I.

The paper is structured as follows. Our problem statements along with the analysis of computational challenges is devoted in Section II, while Section III develops a convex-solver based universal algorithm for their solution. Section IV develops closed-form expression based algorithms of scalable complexity for solving the GM-rate and SR maximizing problem. Followed by Section V, which takes into account realistic antenna-wise power constraints. Our simulations are provided in Section VI, which show that: $(i)$ The convex-solver based and closed-form based algorithms have similar performances, so preference is given to the latter due its practicability in solving large-scale problems of practical interest; $(ii)$ The SR maximization always leads to zero rates for some users, hence it cannot be used for MU OFDM; $(iii)$ GM-rate maximization is not only scalably computable but it is also Pareto optimal in maximizing both SR and WR OFs. Finally, Section VII concludes the paper.

*Notation.* $O_{X\times Y}$ represents a zero matrix of size $X\times Y$, and $I_X$ represents the identity matrix of size $X\times X$. $\text{diag}(z)$ represents a diagonal matrix of the size $k\times k$ with $z_1, z_2, \ldots, z_k$ on its diagonal for $z=(z_1,\ldots,z_k)^T$; $[A]^2$ represents $AA^H$, and $\langle A,B\rangle = \text{trace}(A^HB)$ for the matrices $A$ and $B$. Accordingly, $||A|| = \sqrt{\text{trace}(A^HA)}$ is the Frobenius norm of $A$. Only the vector/matrix variables are printed in boldface. To indicate the positive definite (positive semi-definite, resp.) for the Hermitian symmetric matrix $A$, the notation $A\succeq 0$ ($A\succ 0$, resp.) is used. For notational simplicity, we also write $\langle Z\rangle = \text{trace}(Z)$. $\lambda_{\max}(A)$ is used to present the maximal eigenvalue of the Hermitian symmetric matrix $A$. $e^{\jmath z}\triangleq(e^{\jmath z_1},\ldots,e^{\jmath z_k})^T\in\mathbb{C}^k$ for $z=(z_1,\ldots,z_k)^T\in\mathbb{R}^k$. $\angle z$ denotes the argument of a complex number $z$, i.e. $z=e^{\jmath\angle z}$ for $|z|=1$ and it is fully characterized by $\angle z\in[0,2\pi)$. $F_M$ is the fast Fourier transform (FFT) matrix of order $M$ defined as

$$F_M \triangleq \frac{1}{\sqrt{M}}[e^{-\jmath 2\pi kp/M}]_{k,p=0,1,\ldots,M-1}.$$

Note that $F_M$ is unitary ($F_MF_M^H=I_M$) so $F_M^H=(F_M)^{-1}$ is called the inverse FFT (IFFT) matrix.

*Ingredient.* For all $\mathbf{p}\in\mathbb{C}$, $\mathbf{q}>0$, and $\bar{p}\in\mathbb{C}$, $\bar{q}>0$, the following inequality [29] is frequently used:

$$\ln\left(1+\frac{|\mathbf{p}|^2}{\mathbf{q}}\right) \geq \ln\left(1+\frac{|\bar{p}|^2}{\bar{q}}\right)-\frac{|\bar{p}|^2}{\bar{q}}+2\frac{\Re\{\bar{p}^*\mathbf{p}\}}{\bar{q}} -\frac{|\bar{p}|^2}{\bar{q}(|\bar{p}|^2+\bar{q})}(|\mathbf{p}|^2+\mathbf{q}). \quad (1)$$

By considering both sides of (1) as functions of $(\mathbf{p},\mathbf{q})$, it can be observed that the right hand side (RHS) of (1) matches its left hand side (LHS) at $(\bar{p},\bar{q})$. Consequently, the LHS of (1) serves as a tight minorant of the RHS of (1) [30]. The process of maximizing the RHS of (1) is known as tight minorant maximization, which helps to find a better point than that at $(\bar{p},\bar{q})$ in order to maximize the LHS of (1).

## II. Problem Statement

A RIS-aided communication system illustrated by Fig. 1 is considered. Due to having no direct links between the $K$ users (UEs) $k\in\mathcal{K}\triangleq\{1,\ldots,K\}$ equipped with single-antenna and $N_t$-antenna array BS, the RIS of $N$ PREs , which is in direct view of by both the BS and of the UEs is employed to support their downlink.[1]

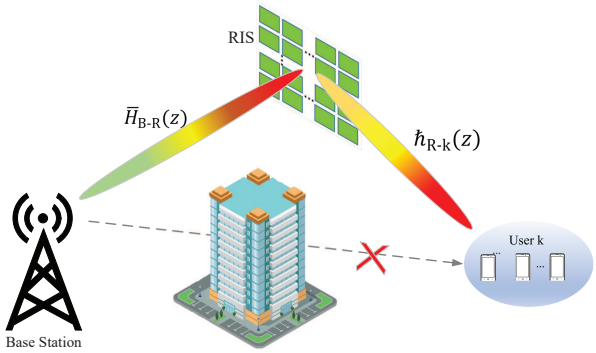


Fig. 1: System model

The channel spanning from the BS to the RIS is assumed to be frequency selective, which is characterized by the transfer co-vector function of

$$\bar{H}_{\text{B-R}}(z)\triangleq\sum_{\ell=0}^{L_1-1}\tilde{H}_{\text{B-R},\ell}z^{-\ell}, \quad (2)$$

where $\tilde{H}_{\text{B-R},\ell}\in\mathbb{C}^{N\times N_t}$ denotes the gain of the $\ell$-th multiple-input multiple-output (MIMO) path and $L_1$ is the memory of the BS-RIS channel.

[1]Between BS and UEs, if the direct link exists, RISs are only marginally useful [9], [11]

TABLE I: Contrasting our novel contributions to the related OFDM literature.

| Contents \ Literature | **This work** | [18]–[20] | [23], [24] | [25] | [26] |
|---|---|---|---|---|---|
| MU OFDM | √ | √ | √ | √ | √ |
| RIS aided single user OFDM | | √ | | | |
| RIS aided MU OFDM | √ | | | | √ |
| SR maximization | √ | | √ | √ | √ |
| WR maximization | √ | | | | |
| Multi-objective optimization | √ | | | | |
| Quantized PREs | √ | | | | |
| Computationally tractable solution | √ | | | | |

Similarly, the channel between the RIS and UE $k$ is also assumed to be frequency-selective and characterized by the transfer co-vector function

$$\hbar_{\text{R-k}}(z) \triangleq \sum_{\ell=0}^{L_2-1} \tilde{h}_{\text{R-k},\ell} z^{-\ell}, \tag{3}$$

where $\tilde{h}_{\text{R-k},\ell} \in \mathbb{C}^{1\times N}$ denotes the gain of the $\ell$-th MISO path and $L_2$ is the memory of the RIS-UE channel.

Let $\mathsf{diag}(e^{\jmath\boldsymbol{\theta}})$ represent the matrix of PREs for $\boldsymbol{\theta} = (\boldsymbol{\theta}_1, \ldots, \boldsymbol{\theta}_N)^T \in [0, 2\pi)^N$. We are concerned about quantized PREs with $b$-bit resolution, formulated as:

$$\boldsymbol{\theta}_n \in \mathcal{B} \triangleq \{\eta \frac{2\pi}{2^b}, \eta = 0, 1, \ldots, 2^b - 1\}, n \in \mathcal{N} \triangleq \{1, \ldots, N\}. \tag{4}$$

Then, the projection of $\alpha \in [0, 2\pi]$ into $\mathcal{B}$ denoted by $\lfloor \alpha \rceil_b$ is termed as its $b$-bit rounded value, i.e.

$$\lfloor \alpha \rceil_b = \eta_\alpha \frac{2\pi}{2^b} \tag{5}$$

with

$$\eta_\alpha \triangleq \arg \min_{\eta=0,1,\ldots,2^b-1} \left| \eta \frac{2\pi}{2^b} - \alpha \right|, \tag{6}$$

which can be easily obtained, because $\eta_\alpha \in \{\eta, \eta+1\}$ for $\alpha \in [\eta \frac{2\pi}{2^b}, (\eta+1)\frac{2\pi}{2^b}]$. When $b = \infty$, have:

$$\alpha = \lfloor \alpha \rceil_\infty. \tag{7}$$

The composite channel spanning from the BS to UE $k$ is also frequency selective and characterized by the transfer co-vector function

$$\begin{aligned} \hbar_k(z) &= \hbar_{\text{R-k}}(z) \mathcal{R}_{\text{R-k}}^{1/2} \mathsf{diag}(e^{\jmath\boldsymbol{\theta}}) \bar{H}_{\text{B-R}}(z) & (8) \\ &= \hbar_{\text{BR-k}}(z) \mathsf{diag}(e^{\jmath\boldsymbol{\theta}}) H_{\text{B-R}}(z) \in \mathbb{C}^{1\times N_t}, & (9) \end{aligned}$$

with

$$\hbar_{\text{BR-k}}(z) \triangleq \sqrt{\beta_{\text{B-R}}} \sqrt{\beta_{\text{R-k}}} h_{\text{R-k}}(z) \mathcal{R}_{\text{R-k}}^{1/2} \in \mathbb{C}^{1\times N}. \tag{10}$$

where $\mathcal{R}_{\text{R-k}} \in \mathbb{C}^{N\times N}$ denotes the spatial correlation matrix, which models the correlation between the RIS elements with respect to user $k$ [31]. In this paper, we adopt a simple exponential model to describe the spatial correlation among the scattering elements of the RIS [32], [33]. Similarly to the seminal papers on RIS-aided communication networks [15], [34]–[38], we assume having perfect channel state information, which can be acquired using the channel estimation techniques created for RIS-aided networks [39]–[44].

Assume that we have $M = 2^{\mathcal{M}}$ sub-carriers. At the $i$-th transmit antenna (TA) $i \in \mathcal{N}_t \triangleq \{1, \ldots, N_t\}$, each block of information

$$x_i \triangleq \begin{bmatrix} x_i(0) \\ \ldots \\ x_i(M-1) \end{bmatrix},$$

of length $M$ is transmitted by OFDM having the block length of $M + L$:

$$\tilde{x}_i \triangleq \begin{bmatrix} x_{i,T} \\ x_{i,H} \\ x_{i,T} \end{bmatrix} \in \mathbb{C}^{M+L}$$

with

$$\begin{bmatrix} x_{i,H} \\ x_{i,T} \end{bmatrix} = F_M^H x_i, x_{i,H} \in \mathbb{C}^{M-L}, x_{i,T} \in \mathbb{C}^L,$$

where the OFDM cyclic prefix (CP) length is set to $L \geq \max\{L_1 + L_2 - 1, L_3\}$ to avoid inter-block interference (IBI). The block $\tilde{x}_i$ of length $(M + L)$ is transmitted from the $i$-th TA. By discarding the first $L$ entries of the received block and then applying the FFT, we obtain the received singal at each subcarrier $m \in \mathcal{M} \triangleq \{0, \ldots, M-1\}$ for UE $k$ as

$$y_k(m) = \hbar_{k,m}(\boldsymbol{\theta}) x(m) + n_k(m), \tag{11}$$

where we have:

$$x(m) \triangleq \begin{bmatrix} x_1(m) \\ \ldots \\ x_{N_t}(m) \end{bmatrix} \in \mathbb{C}^{N_t}, \tag{12}$$

and $n_k(m)$ is the background noise of power $\sigma$, and

$$\begin{aligned} \hbar_{k,m}(\boldsymbol{\theta}) &= \hbar_k(e^{\jmath 2\pi m/M}) & (13) \\ &= \hbar_{\text{BR-k,m}} \mathsf{diag}(e^{\jmath\boldsymbol{\theta}}) H_{\text{B-R,m}} & (14) \end{aligned}$$

with

$$H_{\text{B-R,m}} \triangleq H_{\text{B-R}}(e^{\jmath 2\pi m/M}). \tag{15}$$

$$\hbar_{\text{BR-k,m}} \triangleq \hbar_{\text{BR-k}}(e^{\jmath 2\pi m/M}). \tag{16}$$

In MU beamforming, each $x(m) \in \mathbb{C}^{N_t}$ in (12) is defined as

$$x(m) = \sum_{k=1}^{K} \mathbf{w}_k(m) s_k(m), \tag{17}$$

where $s_k(m) \in \mathcal{C}(0, 1)$ is the data symbol of UE $k$, and its beamformer is

$$\mathbf{w}_k(m) \triangleq \begin{bmatrix} \mathbf{w}_{k,1}(m) \\ \ldots \\ \mathbf{w}_{k,N_t}(m) \end{bmatrix} \in \mathbb{C}^{N_t}, k \in \mathcal{K}. \tag{18}$$

Thus, the received signal in (11) becomes

$$y_k(m) = \hbar_{k,m}(\boldsymbol{\theta}) \sum_{j=1}^{K} \mathbf{w}_j(m) s_j(m) + n_k(m). \quad (19)$$

Let

$$\mathbf{w}(m) \triangleq \begin{bmatrix} \mathbf{w}_1(m) \\ \dots \\ \mathbf{w}_K(m) \end{bmatrix} \in \mathbb{C}^{KN_t},$$

and $\mathbf{w} \triangleq \{\mathbf{w}(m), m \in \mathcal{M}\}$. The rate in nats/sec of $s_k(m)$ for UE $k$ is

$$r_{k,m}(\mathbf{w}(m), \boldsymbol{\theta}) = \ln\left(1 + \frac{|\hbar_{k,m}(\boldsymbol{\theta})\mathbf{w}_k(m)|^2}{\sum_{j \in \mathcal{K}\setminus\{k\}} |\hbar_{k,m}(\boldsymbol{\theta})\mathbf{w}_j(m)|^2 + \sigma}\right). \quad (20)$$

The total rate of UE $k$ is

$$\rho_k(\mathbf{w}, \boldsymbol{\theta}) \triangleq \sum_{m=0}^{M-1} r_{k,m}(\mathbf{w}(m), \boldsymbol{\theta}), \quad (21)$$

while the total information delivery over the subcarrier $m$ is

$$\chi_m(\mathbf{w}(m), \boldsymbol{\theta}) \triangleq \sum_{k=1}^{K} r_{k,m}(\mathbf{w}(m), \boldsymbol{\theta}). \quad (22)$$

Let $P$ denote the total transmit power budget, the power constraint is

$$(1 + \frac{L}{M}) \sum_{k=1}^{K} \sum_{m=0}^{M-1} ||\mathbf{w}_k(m)||^2 \leq P. \quad (23)$$

Let us define the vector-valued function

$$\rho(\mathbf{w}, \boldsymbol{\theta}) \triangleq [\rho_1(\mathbf{w}, \boldsymbol{\theta}), \dots, \rho_K(\mathbf{w}, \boldsymbol{\theta})]^T. \quad (24)$$

As regards to the joint design of the beamformer $\mathbf{w}$ and the PREs $\boldsymbol{\theta}$, the following problems are popular: the SR problem

$$\max_{\mathbf{w}, \boldsymbol{\theta}} f_{SR}[\rho(\mathbf{w}, \boldsymbol{\theta})] \triangleq \sum_{k=1}^{K} \rho_k(\mathbf{w}, \boldsymbol{\theta}) \quad \text{s.t.} \quad (4), (23), \quad (25)$$

and the WR problem

$$\max_{\mathbf{w}, \boldsymbol{\theta}} f_{WR}[\rho(\mathbf{w}, \boldsymbol{\theta})] \triangleq \min_{k=1,\dots,K} \rho_k(\mathbf{w}, \boldsymbol{\theta}) \quad \text{s.t.} \quad (4), (23), \quad (26)$$

which has not been considered even in the RIS-less OFDM literature due to its computational intractability. In addition to the SR problem (25) and WR problem (26), we also consider the GM-rate optimization problem

$$\max_{\mathbf{w}, \boldsymbol{\theta}} f_{GM}(\rho(\mathbf{w}, \boldsymbol{\theta})) \triangleq \left(\prod_{k=1}^{K} \rho_k(\mathbf{w}, \boldsymbol{\theta})\right)^{1/K} \quad \text{s.t.} \quad (4), (23). \quad (27)$$

Our previous treatises [11], [12], [45] have shown that GM-rate maximization leads to a Pareto optimal solution in optimizing both the WR and SR.

All these problems constitute large scale mixed discrete continuous optimization problem with unknown computational solution. The next sections are devoted to their computation.

## III. Universal convex solver based algorithms

This section provides a new penalty optimization based method is conceived for solving the problems (25), (26), and (27) in unified framework by exploiting the fact that the OF $f_A(\rho)$ associated with $A \in \{SR, WR, GM\}$ are concave and monotonically increasing in $\rho$. Let $\hbar_{k,m}(\mathbf{z})$ ($\rho_{k,m}(\mathbf{w}(m), \mathbf{z})$, resp.) be defined from (14) ((21), resp.) with with $e^{\jmath\boldsymbol{\theta}}$ replaced by $\mathbf{z}$. We address (25), (26), and (27) inform of the following penalty optimization problem

$$\max_{\mathbf{w}, \boldsymbol{\theta}, \mathbf{z}} f_A^c(\mathbf{w}, \boldsymbol{\theta}, \mathbf{z}) \triangleq f_A[\rho(\mathbf{w}, \mathbf{z})] - c||\mathbf{z} - e^{\jmath\boldsymbol{\theta}}||^2 \quad \text{s.t.} \quad (4), (23), \quad (28)$$

where $c > 0$ is a penalty parameter, and $A \in \{SR, WR, GM\}$. Note that the discrete constraint (4) prevents us from exploiting the exact penalty optimization of [9].

Assuming an initial feasible point $(w^{(0)}, \theta^{(0)}, z^{(0)})$ for (28), let $(w^{(\iota)}, \theta^{(\iota)}, z^{(\iota)})$ denotes its feasible point, obtained from the $(\iota - 1)$-st iteration.

### A. Beamforming alternating iteration

We seek $w^{(\iota+1)}$, so that the following holds:

$$\begin{aligned} & f_A^c(w^{(\iota+1)}, \theta^{(\iota)}, z^{(\iota)}) > f_A^c(w^{(\iota)}, \theta^{(\iota)}, z^{(\iota)}) \\ \Leftrightarrow \quad & f_A[\rho(w^{(\iota+1)}, z^{(\iota)})] > f_A[\rho(w^{(\iota)}, z^{(\iota)})]. \end{aligned} \quad (29)$$

By using the inequality (1) for $\mathbf{p} = \hbar_{k,m}(z^{(\iota)})\mathbf{w}_k(m)$, $\mathbf{q} = \sum_{j \in \mathcal{K}\setminus\{k\}} |\hbar_{k,m}(z^{(\iota)})\mathbf{w}_j(m)|^2 + \sigma$, and $\bar{p} = \hbar_{k,m}(z^{(\iota)})w_k^{(\iota)}(m)$, $\bar{q} = q_{k,m}^{(\iota)} \triangleq \sum_{j \in \mathcal{K}\setminus\{k\}} |\hbar_{k,m}(z^{(\iota)})w_j^{(\iota)}(m)|^2 + \sigma$, the following tight concave minorant of $r_{k,m}(\mathbf{w}(m), z^{(\iota)})$ at $w^{(\iota)}(m)$ is obtained:

$$\begin{aligned} r_{k,m}^{(\iota)}(\mathbf{w}(m)) \quad \triangleq \quad & a_{k,m}^{(\iota)} + 2\Re\{\langle b_{k,m}^{(\iota)}, \mathbf{w}_k(m)\rangle\} \\ & - c_{k,m}^{(\iota)} \sum_{j=1}^{K} |\hbar_{k,m}(z^{(\iota)})\mathbf{w}_j(m)|^2, \end{aligned} \quad (30)$$

with

$$\begin{aligned} a_{k,m}^{(\iota)} &\triangleq r_{k,m}(\theta^{(\iota)}, w^{(\iota)}(m)) - \frac{|\hbar_{k,m}(z^{(\iota)})w_k^{(\iota)}(m)|^2}{y_{k,m}^{(\iota)}} - \sigma c_{k,m}^{(\iota)}, \\ b_{k,m}^{(\iota)} &\triangleq \frac{\hbar_{k,m}(z^{(\iota)})w_k^{(\iota)}(m)}{y_{k,m}^{(\iota)}} \hbar_{k,m}^H(z^{(\iota)}), \\ 0 < c_{k,m}^{(\iota)} &\triangleq \frac{|\hbar_{k,m}(z^{(\iota)})w_{k,m}^{(\iota)}|^2}{y_{k,m}^{(\iota)}\left(y_{k,m}^{(\iota)} + |\hbar_{k,m}(z^{(\iota)})w_k^{(\iota)}(m)|^2\right)}. \end{aligned} \quad (31)$$

By defining the following tight concave minorant of $\rho_k(\mathbf{w}, z^{(\iota)})$ at $w^{(\iota)}$:

$$\rho_k^{(\iota)}(\mathbf{w}) \triangleq \sum_{m=0}^{M-1} r_{k,m}^{(\iota)}(\mathbf{w}(m)), \quad (32)$$

and then $\rho^{(\iota)}(\mathbf{w}) \triangleq [\rho_1^{(\iota)}(\mathbf{w}), \dots, \rho_K(\mathbf{w})]^T$, we obtain $f_A[\rho^{(\iota)}(\mathbf{w})]$ as a tight minorant of $f_A[\rho(\mathbf{w}, z^{(\iota)})]$ at $w^{(\iota)}$. Thus, we generate $w^{(\iota+1)}$ at the $\iota$-th iteration by solving the following problem:

$$\max_{\mathbf{w}} \; f_A[\rho^{(\iota)}(\mathbf{w})] \quad \text{s.t.} \quad (23). \quad (33)$$

Note that $f_A[\rho^{(\iota)}(\mathbf{w})]$ is either a concave function as a sum or pointwise minimum or alternatively the GM of concave functions $\rho_k^{(\iota)}(\mathbf{w})$ [30], so this problem is convex.

### B. z-iteration

We look for the next iterative point $z^{(\iota+1)}$, which should ensure

$$\begin{aligned} & f_A^c(w^{(\iota+1)},\theta^{(\iota)},z^{(\iota+1)}) > f_A^c(w^{(\iota+1)},\theta^{(\iota)},z^{(\iota)}) \quad (34)\\ \Leftrightarrow \quad & f_A(\rho(w^{(\iota+1)},z^{(\iota+1)})) - c||z^{(\iota+1)} - e^{\jmath\theta^{(\iota)}}||^2 > \\ & f_A(\rho(w^{(\iota+1)},z^{(\iota)}) - c||z^{(\iota)} - e^{\jmath\theta^{(\iota)}}||^2. \end{aligned}$$

By using the inequality (1) with $\mathbf{p} = \hbar_{k,m}(\mathbf{z})w_k^{(\iota+1)}(m)$, $\mathbf{q} = \sum_{j\in\mathcal{K}\setminus\{k\}} |\hbar_{k,m}(\mathbf{z})w_j^{(\iota+1)}(m)|^2 + \sigma$, and $\bar{p} = \hbar_{k,m}(z^{(\iota)})w_k^{(\iota+1)}(m)$, $\bar{q} = q_{k,m}^{(\iota+1)} \triangleq \sum_{j\in\mathcal{K}\setminus\{k\}} |\hbar_{k,m}(z^{(\iota)})w_j^{(\iota+1)}(m)|^2 + \sigma$, we obtain the following tight concave minorant of $r_{k,m}(w^{(\iota+1)},\mathbf{z})$ at $z^{(\iota)}$:

$$\begin{aligned} \tilde{r}_{k,m}^{(\iota)}(\mathbf{z}) \quad \triangleq \quad & \tilde{a}_{k,m}^{(\iota)} + \frac{2}{y_{k,m}^{(\iota+1)}}\Re\{\tau_{k,m}^{(\iota)}\hbar_{k,m}(\boldsymbol{\theta})w_k^{(\iota+1)}(m)\} \\ & -\tilde{c}_{k,m}^{(\iota)}\sum_{j=1}^{K}|\hbar_{k,m}(\boldsymbol{\theta})w_j^{(\iota+1)}(m)|^2, \end{aligned} \quad (35)$$

with

$$\tau_{k,m}^{(\iota)} \triangleq (\hbar_{k,m}(z^{(\iota)})w_k^{(\iota+1)}(m))^* \in \mathbb{C},$$

and

$$\begin{aligned} \tilde{a}_{k,m}^{(\iota)} \quad \triangleq \quad & r_{k,m}(w^{(\iota+1)},z^{(\iota)}) - \sigma\tilde{c}_{k,m}^{(\iota)} \\ & -\frac{|\hbar_{k,m}(z^{(\iota)})w_k^{(\iota+1)}(m)|^2}{y_{k,m}^{(\iota+1)}}, \end{aligned}$$

$$0 < \tilde{c}_{k,m}^{(\iota)} \triangleq \frac{|\hbar_{k,m}(z^{(\iota)})w_k^{(\iota+1)}(m)|^2}{y_{k,m}^{(\iota+1)}\left(y_{k,m}^{(\iota+1)} + |\hbar_{k,m}(z^{(\iota)})w_k^{(\iota+1)}(m)|^2\right)}.$$

Thus, a tight concave minorant of $\rho_k(w^{(\iota+1)},\mathbf{z})$ at $z^{(\iota)}$ is

$$\tilde{\rho}_k^{(\iota)}(\mathbf{z}) \triangleq \sum_{m=0}^{M-1}\tilde{r}_{k,m}^{(\iota)}(\mathbf{z}), \quad (36)$$

and a tight concave minorant of $f_A(w^{(\iota+1)},\mathbf{z})$ at $z^{(\iota)}$ is $f_A[\tilde{\rho}^{(\iota)}(\mathbf{z})]$ for $\tilde{\rho}^{(\iota)}(\mathbf{z}) \triangleq [\tilde{\rho}_1^{(\iota)}(\mathbf{z}),\ldots,\tilde{\rho}_K^{(\iota)}(\mathbf{z})]^T$. Thus, we generate $z^{(\iota+1)}$ by solving the following convex problem, which verifies (34):

$$\max_{\mathbf{z}} \; f_A[\tilde{\rho}_1^{(\iota)}(\mathbf{z}),\ldots,\tilde{\rho}_K^{(\iota)}(\mathbf{z})] - c||\mathbf{z} - e^{\jmath\theta^{(\iota)}}||^2, \quad (37)$$

### C. PREs iteration

We generate $\theta^{(\iota+1)}$ so that $f_A^c(w^{(\iota+1)},\theta^{(\iota+1)},z^{(\iota+1)}) > f_A^c(w^{(\iota+1)},\theta^{(\iota)},z^{(\iota+1)}) \Leftrightarrow -||z^{(\iota+1)} - e^{\jmath\boldsymbol{\theta}}||^2 > -||z^{(\iota)} - e^{\jmath\boldsymbol{\theta}}||^2$ by solving

$$\max_{\boldsymbol{\theta}} -||z^{(\iota+1)} - e^{\jmath\boldsymbol{\theta}}||^2 \quad \text{s.t.} \quad (4), \quad (38)$$

the closed-form solution is obtained:

$$\theta_n^{(\iota+1)} = \lfloor z_n^{(\iota+1)}\rceil_b, n \in \mathcal{N}. \quad (39)$$

**Algorithm 1** SR, WR, GM-rate optimization

1: **Initialization:** Set $\iota = 0$. Generate a random feasible $(w^{(0)},\theta^{(0)},z^{(0)})$ for (28).
2: **Repeat until convergence of the OF in** (28)**:** Calculate $w^{(\iota+1)}$ by solving (33), $z^{(\iota+1)}$ by solving (37), and $\theta^{(\iota+1)}$ by (39). Reset $\iota = \iota + 1$.
3: **Output** $(w^{(\iota)},\theta^{(\iota)})$ and the user rates $\rho_k(w^{(\iota)},\theta^{(\iota)})$, $k \in \mathcal{K}$.

### D. Algorithm and convergene

Based on (33), (37) and (39), the pseudo-code to generate a sequence of $\{(w^{(\iota)},z^{(\iota)},\theta^{(\iota)})\}$ is provided in Algorithm 1 so that

$$f_A^c(w^{(\iota+1)},z^{(\iota+1)},\theta^{(\iota+1)}) > f_A^c(w^{(\iota)},z^{(\iota)},\theta^{(\iota)}), \quad (40)$$

which is convergent according to the Cauchy theorem.

## IV. Closed-form expression based algorithms for GM-rate and SR maximization

The computational complexity of the convex problems (33) and (37) is on the order of $\mathcal{O}[(KN_tM)^3]$ and $\mathcal{O}(N^3)$, respectively. Therefore, the computational complexity of each iteration of Algorithm 1's is $\mathcal{O}[(KN_tM)^3)+\mathcal{O}(N^3]$, which is excessive since both $M$ and $N$ are large in real applications. This section presents algorithms of scalable complexity for solving the SR problem (25) and GM-rate problem (27) by leveraging the smoothness of their objective functions.

The problem (27) is considered first. Starting from some initial feasible point $(w^{(0)},\theta^{(0)})$ of (27), let $(w^{(\iota)},\theta^{(\iota)})$ be its feasible point obtained from the $(\iota-1)$-st iteration. For the nonlinear vector function $\rho(\mathbf{w},\boldsymbol{\theta})$ defined from (24), the linearized function of the composite $f_{GM}[\rho(\mathbf{w},\boldsymbol{\theta})]$ at $\rho(w^{(\iota)},\theta^{(\iota)})$ is defined by[2]

$$\mathcal{L}^{(\iota)}(\rho(\mathbf{w},\mathbf{z})) \triangleq \frac{f_{GM}[\rho(w^{(\iota)},\theta^{(\iota)})]}{K}\sum_{k=1}^{K}\frac{\rho_k(\mathbf{w},\boldsymbol{\theta})}{\rho_k(w^{(\iota)},\theta^{(\iota)})}. \quad (41)$$

At the $\iota$-th iteration, we seek a steep ascent $(w^{(\iota+1)},\theta^{(\iota+1)})$ by considering the following problem:

$$\max_{\mathbf{w},\boldsymbol{\theta}} \mathcal{L}^{(\iota)}[\rho(\mathbf{w},\mathbf{z})] \quad \text{s.t.} \quad (4),(23), \quad (42)$$

which is equivalent to the following problem of weighted SR maximization,

$$\max_{\mathbf{w},\boldsymbol{\theta}} f^{(\iota)}(\mathbf{w},\boldsymbol{\theta}) \triangleq \sum_{k=1}^{K}\gamma_k^{(\iota)}\rho_k(\mathbf{w},\boldsymbol{\theta}) \quad \text{s.t.} \quad (4),(23), \quad (43)$$

for

$$\gamma_k^{(\iota)} \triangleq \frac{\max_{k'\in\mathcal{K}}\rho_{k'}(w^{(\iota)},\theta^{(\iota)})}{\rho_k(w^{(\iota)},\theta^{(\iota)})}, k \in \mathcal{K}. \quad (44)$$

[2]The derivation process is given in [11, Section II, Eq(7-12)]

### A. Beamforming alternating iteration

To seek $w^{(\iota+1)}$, so that the following holds:

$$f^{(\iota)}(w^{(\iota+1)},\theta^{(\iota)}) > f^{(\iota)}(w^{(\iota)},\theta^{(\iota)}), \tag{45}$$

we address the following problem

$$\max_{\mathbf{w}} f^{(\iota)}(\mathbf{w},\theta^{(\iota)}) \triangleq \sum_{k=1}^{K}\gamma_k^{(\iota)}\rho_k(\mathbf{w},\theta^{(\iota)}) \quad \text{s.t.} \quad (23). \tag{46}$$

By using the inequality (1) for $\mathbf{p} = \hbar_{k,m}(\theta^{(\iota)})\mathbf{w}_k(m)$, $\mathbf{q} = \sum_{j\in\mathcal{K}\setminus\{k\}}|\hbar_{k,m}(\theta^{(\iota)})\mathbf{w}_j(m)|^2 + \sigma$, and $\bar{p} = \hbar_{k,m}(\theta^{(\iota)})w_k^{(\iota)}(m)$, $\bar{q} = q_{k,m}^{(\iota)} \triangleq \sum_{j\in\mathcal{K}\setminus\{k\}}|\hbar_{k,m}(\theta^{(\iota)})w_j^{(\iota)}(m)|^2+\sigma$, we obtain the following concave tight minorant of $r_{k,m}(\mathbf{w}(m),\theta^{(\iota)})$ at $w^{(\iota)}(m)$:

$$\begin{aligned} r_{k,m}^{(\iota)}(\mathbf{w}(m)) &\triangleq a_{k,m}^{(\iota)} + 2\Re\{\langle b_{k,m}^{(\iota)},\mathbf{w}_k(m)\rangle\} \\ &\quad -c_{k,m}^{(\iota)}\sum_{j=1}^{K}|\hbar_{k,m}(\theta^{(\iota)})\mathbf{w}_j(m)|^2, \end{aligned} \tag{47}$$

with

$$\begin{aligned} a_{k,m}^{(\iota)} &\triangleq r_{k,m}(\theta^{(\iota)},w^{(\iota)}(m)) - \frac{|\hbar_{k,m}(\theta^{(\iota)})w_k^{(\iota)}(m)|^2}{y_{k,m}^{(\iota)}} - \sigma c_{k,m}^{(\iota)}, \\ b_{k,m}^{(\iota)} &\triangleq \frac{\hbar_{k,m}(\theta^{(\iota)})w_k^{(\iota)}(m)}{y_{k,m}^{(\iota)}}\hbar_{k,m}^{H}(\theta^{(\iota)}), \\ 0 < c_{k,m}^{(\iota)} &\triangleq \frac{|\hbar_{k,m}(\theta^{(\iota)})w_{k,m}^{(\iota)}|^2}{y_{k,m}^{(\iota)}\left(y_{k,m}^{(\iota)}+|\hbar_{k,m}(\theta^{(\iota)})w_k^{(\iota)}(m)|^2\right)}. \end{aligned} \tag{48}$$

Thus, a tight concave minorant of $f^{(\iota)}(\mathbf{w},\theta^{(\iota)})$ at $w^{(\iota)}$ is given by:

$$\begin{aligned} f_b^{(\iota)}(\mathbf{w}) &\triangleq \sum_{k=1}^{K}\gamma_k^{(\iota)}\sum_{m=0}^{M-1}r_{k,m}^{(\iota)}(\mathbf{w}(m)) \\ &= \sum_{k=1}^{K}\gamma_k^{(\iota)}\sum_{m=0}^{M-1}a_{k,m}^{(\iota)} \\ &\quad +2\sum_{k=1}^{K}\gamma_k^{(\iota)}\sum_{m=0}^{M-1}\Re\{\langle b_{k,m}^{(\iota)},\mathbf{w}_k(m)\rangle\} \\ &\quad -\sum_{m=0}^{M-1}\sum_{k=1}^{K}\mathbf{w}_k^{H}(m)\Psi_m^{(\iota)}\mathbf{w}_k(m) \end{aligned} \tag{49}$$

with

$$0 \preceq \Psi_m^{(\iota)} \triangleq \sum_{j=1}^{K}\gamma_j^{(\iota)}c_{j,m}^{(\iota)}\hbar_{j,m}^{H}(\theta^{(\iota)})\hbar_{j,m}(\theta^{(\iota)}), m\in\mathcal{M}. \tag{50}$$

Thus, $w^{(\iota+1)}$ verifying (45) can be sought as the optimal solution of the following convex problem of tight minorant maximization of (46)

$$\max_{\mathbf{w}} f_b^{(\iota)}(\mathbf{w}) \quad \text{s.t.} \quad (23), \tag{51}$$

which results in the following closed-form solution:

$$w_k^{(\iota+1)}(m) = \begin{cases} \gamma_k^{(\iota)}(\Psi_m^{(\iota)})^{-1}b_{k,m}^{(\iota)} \\ \text{if}(1+\frac{L}{M})\sum_{m=0}^{M-1}\sum_{k=1}^{K}||\gamma_k^{(\iota)}(\Psi_m^{(\iota)})^{-1}b_{k,m}^{(\iota)}||^2 \le P \\ \gamma_k^{(\iota)}(\Psi_m^{(\iota)}+\mu I_{N_t})^{-1}b_{k,m}^{(\iota)} \qquad \text{otherwise}, \end{cases} \tag{52}$$

where $\mu > 0$ is chosen by bisection so that

$$(1+\frac{L}{M})\sum_{m=0}^{M-1}\sum_{k=1}^{K}||\gamma_k^{(\iota)}(\Psi_m^{(\iota)}+\mu I_{N_t})^{-1}b_{k,m}^{(\iota)}||^2 = P. \tag{53}$$

### B. PREs' alternating iteration

The next iterative point $\theta^{(\iota+1)}$ is sought to satisfy

$$f^{(\iota)}(w^{(\iota+1)},\theta^{(\iota+1)}) > f^{(\iota)}(w^{(\iota+1)},\theta^{(\iota)}), \tag{54}$$

we address the problem

$$\max_{\boldsymbol{\theta}} f^{(\iota)}(w^{(\iota+1)},\boldsymbol{\theta}) \quad \text{s.t.} \quad (4). \tag{55}$$

By using the inequality (1) for $\mathbf{p} = \hbar_{k,m}(\boldsymbol{\theta})w_k^{(\iota+1)}(m)$, $\mathbf{q} = \sum_{j\in\mathcal{K}\setminus\{k\}}|\hbar_{k,m}(\boldsymbol{\theta})w_j^{(\iota+1)}(m)|^2 + \sigma$, and $\bar{p} = \hbar_{k,m}(\theta^{(\iota)})w_k^{(\iota+1)}(m)$, $\bar{q} = q_{k,m}^{(\iota+1)} \triangleq \sum_{j\in\mathcal{K}\setminus\{k\}}|\hbar_{k,m}(\theta^{(\iota)})w_j^{(\iota+1)}(m)|^2 + \sigma$, we obtain the following tight minorant of $r_{k,m}(w^{(\iota+1)},\boldsymbol{\theta})$ at $\theta^{(\iota)}$:

$$\begin{aligned} \tilde{r}_{k,m}^{(\iota)}(\boldsymbol{\theta}) &\triangleq \tilde{a}_{k,m}^{(\iota)} + \frac{2}{y_{k,m}^{(\iota+1)}}\Re\{\tau_{k,m}^{(\iota)}\hbar_{k,m}(\boldsymbol{\theta})w_k^{(\iota+1)}(m)\} \\ &\quad -\tilde{c}_{k,m}^{(\iota)}\sum_{j=1}^{K}|\hbar_{k,m}(\boldsymbol{\theta})w_j^{(\iota+1)}(m)|^2, \end{aligned} \tag{56}$$

with

$$\tau_{k,m}^{(\iota)} \triangleq [\hbar_{k,m}(\theta^{(\iota)})w_k^{(\iota+1)}(m)]^* \in \mathbb{C},$$

and

$$\begin{aligned} \tilde{a}_{k,m}^{(\iota)} &\triangleq r_{k,m}(w^{(\iota+1)},\theta^{(\iota)}) - \frac{|\hbar_{k,m}(\theta^{(\iota)})w_k^{(\iota+1)}(m)|^2}{y_{k,m}^{(\iota+1)}} - \sigma\tilde{c}_{k,m}^{(\iota)}, \\ 0 < \tilde{c}_{k,m}^{(\iota)} &\triangleq \frac{|\hbar_{k,m}(\theta^{(\iota)})w_k^{(\iota+1)}(m)|^2}{y_{k,m}^{(\iota+1)}\left(y_{k,m}^{(\iota+1)}+|\hbar_{k,m}(\theta^{(\iota)})w_k^{(\iota+1)}(m)|^2\right)}. \end{aligned}$$

Then we have:

$$\mathsf{diag}(e^{\jmath\boldsymbol{\theta}}) = \sum_{n=1}^{N}e^{\jmath\boldsymbol{\theta}_n}\Upsilon_n,$$

where $\Upsilon_n$ denotes a matrix of size $(N\times N)$ with only zero entries, except its $(n,n)$-entry is 1.

We then use (14) to arrive at:

$$\begin{aligned} &\tau_{k,m}^{(\iota)}\hbar_{k,m}(\boldsymbol{\theta})w_k^{(\iota+1)}(m) \\ =\ &\tau_{k,m}^{(\iota)}\left[\hbar_{\text{BR-k,m}}\mathsf{diag}(e^{\jmath\boldsymbol{\theta}})H_{\text{B-R,m}}\right]w_k^{(\iota+1)}(m) \\ =\ &\tau_{k,m}^{(\iota)}\sum_{n=1}^{N}\tau_{k,m}^{(\iota)}\hbar_{\text{BR-k,m}}\Upsilon_n H_{\text{B-R,m}}w_k^{(\iota+1)}(m)e^{\jmath\boldsymbol{\theta}_n} \\ =\ &\sum_{n=1}^{N}\tilde{b}_{k,m}^{(\iota)}(n)e^{\jmath\boldsymbol{\theta}_n}, \end{aligned} \tag{57}$$

with [3]

$$\tilde{b}_{k,m}^{(\iota)}(n) = \tau_{k,m}^{(\iota)} \hbar_{\text{BR-k,m}} \Upsilon_n H_{\text{B-R,m}} w_k^{(\iota+1)}(m), n \in \mathcal{N}.$$

To expound further, we have:

$$\begin{aligned} & |\hbar_{k,m}(\boldsymbol{\theta}) w_j^{(\iota+1)}(m)|^2 \\ = & \left| \left( \hbar_{\text{BR-k,m}} \mathsf{diag}(e^{\jmath\boldsymbol{\theta}}) H_{\text{B-R,m}} \right) w_j^{(\iota+1)}(m) \right|^2. \end{aligned} \quad (58)$$

Furthermore,

$$\begin{aligned} & \hbar_{\text{BR-k,m}} \mathsf{diag}(e^{\jmath\boldsymbol{\theta}}) H_{\text{B-R,m}} w_j^{(\iota+1)}(m) \\ = & \hbar_{\text{BR-k,m}} \left( \sum_{n=1}^{N} e^{\jmath\boldsymbol{\theta}_n} \Upsilon_n \right) H_{\text{B-R,m}} w_j^{(\iota+1)}(m) \\ = & \sum_{n=1}^{N} q_{k,m,j}^{(\iota+1)}(n) e^{\jmath\boldsymbol{\theta}_n}, \end{aligned} \quad (59)$$

for

$$q_{k,m,j}^{(\iota+1)}(n) = \hbar_{\text{BR-k,m}} \Upsilon_n H_{\text{B-R,m}} w_j^{(\iota+1)}(m), n \in \mathcal{N}.$$

Based on (56), (57), (58), and (59), we arrive at:

$$\begin{aligned} \tilde{r}_{k,m}^{(\iota)}(\boldsymbol{\theta}) = & \tilde{a}_{k,m}^{(\iota+1)} + 2\Re\{\sum_{n=1}^{N} \tilde{b}_{k,m}^{(\iota+1)}(n) e^{\jmath\boldsymbol{\theta}_n}\} \\ & - \tilde{c}_{k,m}^{(\iota)} \sum_{j=1}^{K} \left| \sum_{n=1}^{N} q_{k,m,j}^{(\iota+1)}(n) e^{\jmath\boldsymbol{\theta}_n} \right|^2 \\ = & \tilde{a}_{k,m}^{(\iota+1)} + 2\Re\{\sum_{n=1}^{N} \tilde{b}_{k,m}^{(\iota+1)}(n) e^{\jmath\boldsymbol{\theta}_n}\} \\ & - \tilde{c}_{k,m}^{(\iota)} \sum_{j=1}^{K} (e^{\jmath\boldsymbol{\theta}})^H \Phi_{k,m,j}^{(\iota+1)} e^{\jmath\boldsymbol{\theta}}, \end{aligned} \quad (60)$$

where

$$\tilde{a}_{k,m}^{(\iota+1)} \triangleq \tilde{a}_{k,m}^{(\iota)} - \tilde{c}_{k,m}^{(\iota)} \sum_{j \in \mathcal{K} \setminus \{k\}} |\hbar_{\text{B-k,m}} w_j^{(\iota+1)}(m)|^2,$$

$$\tilde{d}_{k,m}^{(\iota+1)} \triangleq \sum_{j=1}^{K} \left( \tilde{h}_{\text{B-k,m}} w_j^{(\iota+1)}(m) \right)^* \hbar_{\text{BR-k,m}} \Upsilon_n H_{\text{B-R,m}} w_j^{(\iota+1)}(m),$$

$$\tilde{b}_{k,m}^{(\iota+1)}(n) \triangleq \frac{\tilde{b}_{k,m}^{(\iota)}(n)}{y_{k,m}^{(\iota+1)}} - \tilde{c}_{k,m}^{(\iota)} \tilde{d}_{k,m}^{(\iota+1)}, n \in \mathcal{N}, \quad (61)$$

and

$$\Phi_{k,m,j}^{(\iota+1)}(n,n') = (q_{k,m,j}^{(\iota+1)}(n))^* q_{k,m,j}^{(\iota+1)}(n'), (n,n') \in \mathcal{N} \times \mathcal{N},$$

where we have $\Phi_{k,m,j}^{(\iota+1)} \succeq 0$. Therefore, a tight minorant of the function $f^{(\iota)}(w^{(\iota+1)}, \boldsymbol{\theta})$ at $\theta^{(\iota)}$ is

$$\begin{aligned} f_c^{(\iota)}(\boldsymbol{\theta}) \triangleq & \sum_{k=1}^{K} \gamma_k^{(\iota)} \sum_{m=0}^{M-1} \tilde{r}_{k,m}^{(\iota)}(\boldsymbol{\theta}) \\ = & \tilde{a}^{(\iota+1)} + 2\Re\{\sum_{n=1}^{N} \tilde{b}^{(\iota+1)}(n) e^{\jmath\boldsymbol{\theta}_n}\} \\ & - (e^{\jmath\boldsymbol{\theta}})^H \Phi^{(\iota+1)} e^{\jmath\boldsymbol{\theta}}, \end{aligned} \quad (62)$$

for

$$\begin{aligned} \tilde{a}^{(\iota+1)} \triangleq & \sum_{k=1}^{K} \gamma_{k,m}^{(\iota)} \sum_{m=0}^{M-1} \tilde{a}_{k,m}^{(\iota+1)}, \\ \tilde{b}^{(\iota+1)}(n) \triangleq & \sum_{k=1}^{K} \gamma_k^{(\iota)} \sum_{m=0}^{M-1} \tilde{b}_{k,m}^{(\iota+1)}(n), \\ 0 \preceq \Phi^{(\iota+1)} \triangleq & \sum_{k=1}^{K} \gamma_k^{(\iota)} \sum_{m=0}^{M-1} \tilde{c}_{k,m}^{(\iota)} \sum_{j=1}^{N} \Phi_{k,m,j}^{(\iota+1)}. \end{aligned} \quad (63)$$

Furthermore, (62) may be reformulated as (64), i.e. $\tilde{f}_c^{(\iota)}(\boldsymbol{\theta})$ is a tight minorant of $f_c^{(\iota)}(\boldsymbol{\theta})$ and thus it is still a tight minorant of $f^{(\iota)}(w^{(\iota+1)}, \boldsymbol{\theta})$ at $\theta^{(\iota)}$ [9]. Thus, $\theta^{(\iota+1)}$ satisfying (54) can be sought as the optimal solution of the following problem of tight minorant maximization of (55):

$$\max_{\boldsymbol{\theta} \in \mathcal{B}^N} \ \tilde{f}_c^{(\iota)}(\boldsymbol{\theta}), \quad (65)$$

which admits the closed-form [4] solution of (66).

### C. GM-rate optimization and convergence

The pseudo-code for the proposed procedure of steep descent for computing (27) is provided in Algorithm 2. Instead of seeking the optimal solution of the nonconvex problem (27), we solve the iterations (52) and (66) and seek a descent direction by aiming for a gradually improved feasible point for (27). The rationale of this is reducing the computational load while guaranteeing convergence, and the routine is also used in the Frank-and-Wolfe method [46].

**Algorithm 2** Scalable-complexity GM optimization

1: **Initialization:** Set $\iota = 0$. Generate random $(w^{(0)}, \theta^{(0)})$ meeting the constraint (23) and calculate $\gamma_k^{(0)}$ by (44).
2: **Repeat until convergence of the OF in** (27)**:** Calculate $w^{(\iota+1)}$ by (52) and $\theta^{(\iota+1)}$ by (66). Reset $\iota = \iota + 1$.
3: **Output** $(w^{(\iota)}, \theta^{(\iota)})$ and user rates $\rho_k(w^{(\iota)}, \theta^{(\iota)})$, $k \in \mathcal{K}$.

### D. SR optimization algorithm

The SR problem can also be computed by adapting Algorithm 2 for $\gamma_k^{(\iota)} \equiv 1$ in (43), as it is summarized by Algorithm 3.

**Algorithm 3** Scalable-complexity SR optimization

1: **Initialization:** Set $\iota = 0$. Generate random $(w^{(0)}, \theta^{(0)})$ meeting the constraint (23).
2: **Repeat until convergence of the OF in** (25)**:** Set $\gamma_k^{(\iota)} \equiv 1$ and calculate $w^{(\iota+1)}$ by (52) and $\theta^{(\iota+1)}$ by (66). Reset $\iota = \iota + 1$.
3: **Output** $(w^{(\iota)}, \theta^{(\iota)})$ and the user rates $\rho_k(w^{(\iota)}, \theta^{(\iota)})$, $k \in \mathcal{K}$.

[3] In what follows $b(i)$ is the $i$-th entry of $b$ and $[A](i,i)$ is the $i$-th diagonal entry of $A$, and $[A]^*(i,i)$ is the complex conjugate of $[A](i,i)$

[4] $[(\Phi^{(\iota+1)} - \mu I_N) e^{\jmath\theta^{(\iota)}}](n)$ is the $n$-th entry of $(\Phi^{(\iota+1)} - \mu I_N) e^{\jmath\theta^{(\iota)}}$

$$\begin{aligned} f_c^{(\iota)}(\boldsymbol{\theta}) &= 2\Re\{\sum_{n=1}^{N}\tilde{b}^{(\iota+1)}(n)e^{\jmath\boldsymbol{\theta}_n}\} - (e^{\jmath\boldsymbol{\theta}})^H(\Phi^{(\iota+1)} - \lambda_{\max}(\Phi^{(\iota+1)})I_N)e^{\jmath\boldsymbol{\theta}} + \tilde{a}^{(\iota+1)} - \lambda_{\max}(\Phi^{(\iota+1)})N \\ &\geq \tilde{f}_c^{(\iota)}(\boldsymbol{\theta}) \\ &= 2\Re\{\sum_{n=1}^{N}\left(\tilde{b}^{(\iota+1)}(n) - \sum_{n'=1}^{N} e^{-\jmath\theta_{n'}^{(\iota)}}\Phi^{(\iota+1)}(n',n) + \lambda_{\max}(\Phi^{(\iota+1)})e^{-\jmath\theta_n^{(\iota)}}\right)e^{\jmath\boldsymbol{\theta}_n}\} \\ &\quad +\tilde{a}^{(\iota+1)} - (e^{\jmath\theta^{(\iota)}})^H\Phi^{(\iota+1)}e^{\jmath\theta^{(\iota)}} - 2\lambda_{\max}(\Phi^{(\iota+1)})N, \end{aligned} \tag{64}$$

$$\theta_n^{(\iota+1)} = 2\pi - \lfloor\angle(\tilde{b}^{(\iota+1)}(n) - \sum_{n'=1}^{N} e^{-\jmath\theta_{n'}^{(\iota)}}\Phi^{(\iota+1)}(n',n) + \lambda_{\max}(\Phi^{(\iota+1)})e^{-\jmath\theta_n^{(\iota)}})\rceil_b, n \in \mathcal{N}. \tag{66}$$

## V. Per-antenna power constrained OFDM transmission

In this section we consider the per-antenna power constraints as an alternative for the sum power constraint (23). The per-antenna power-constraints can be expressed as:

$$(1+\frac{L}{M})\sum_{k=1}^{K}\sum_{m=0}^{M-1}|\mathbf{w}_{k,i}(m)|^2 \leq P/N_t, i \in \mathcal{N}_t, \tag{67}$$

under which we concentrate on the GM-rate problem

$$\max_{\mathbf{w},\boldsymbol{\theta}} f_{GM}[\rho(\mathbf{w},\boldsymbol{\theta})] \quad \text{s.t.} \quad (4),(67). \tag{68}$$

Starting from some initial feasible point $(w^{(0)},\theta^{(0)})$ of (68), let $(w^{(\iota)},\theta^{(\iota)})$ be its feasible point obtained from the $(\iota-1)$-st iteration. Accordingly, for $\gamma_k^{(\iota)}$ defined from (44) we iterate the following problem instead of (43):

$$\max_{\mathbf{w},\boldsymbol{\theta}\in\mathcal{B}^N} f^{(\iota)}(\mathbf{w},\boldsymbol{\theta}) \triangleq \sum_{k=1}^{K}\gamma_k^{(\iota)}\rho_k(\mathbf{w},\boldsymbol{\theta}) \quad \text{s.t.} \quad (4),(67). \tag{69}$$

### A. Beamforming alternating iteration

Let $r_{k,m}^{(\iota)}(\mathbf{w}(m))$ be defined from (56), which is a tight minorant of $r_{k,m}(\mathbf{w}(m),\theta^{(\iota)})$. Then, a tight minorant of $f^{(\iota)}(\mathbf{w},\theta^{(\iota)})$ at $w^{(\iota)}$ is defined by

$$f_b^{(\iota)}(\mathbf{w}) \triangleq \sum_{m=0}^{M-1} f_{b,m}^{(\iota)}(\mathbf{w}(m)), \tag{70}$$

where we have

$$\begin{aligned} f_{b,m}^{(\iota)}(\mathbf{w}(m)) &\triangleq \sum_{k=1}^{K}\gamma_k^{(\iota)}r_{k,m}^{(\iota)}(\mathbf{w}(m)) \qquad (71)\\ &= \sum_{k=1}^{K}\gamma_k^{(\iota)}a_{k,m}^{(\iota)} - \sum_{k=1}^{K}\mathbf{w}_k^H(m)\Psi_m^{(\iota)}\mathbf{w}_k(m) \\ &\quad +2\sum_{k=1}^{K}\Re\{\langle\gamma_k^{(\iota)}b_{k,m}^{(\iota)},\mathbf{w}_k(m)\rangle\} \end{aligned}$$

with $a_{k,m}^{(\iota)}$, $b_{k,m}^{(\iota)}$, $c_{k,m}^{(\iota)}$ and $\Psi_m^{(\iota)} \succeq 0$ defined by (48) and (50). Upon considering the last term in the RHS of (71), we used the fact that $\sum_{k=1}^{K}\mathbf{w}_k^H(m)\left(\lambda^{(\iota)}I_{N_t} - \Psi_m^{(\iota)}\right)\mathbf{w}_k(m)$ in (72) is convex quadratic in obtaining (73) from (72).

Therefore, we have (75) and (78). The function $\tilde{f}_{b,m}^{(\iota)}(\mathbf{w})$ is still a tight minorant of $f^{(\iota)}(\mathbf{w},\theta^{(\iota)})$. Hence the following problem is solved to generate $w^{(\iota+1)}$ verifying (45)

$$\max_{\mathbf{w}} \sum_{m=0}^{M-1}\tilde{f}_{b,m}^{(\iota)}(\mathbf{w}(m)) \quad \text{s.t.} \quad (67). \tag{81}$$

Let

$$d_k(m) \triangleq \begin{bmatrix} d_{k,1}(m) \\ \dots \\ d_{k,N_t}(m) \end{bmatrix} = \gamma_k^{(\iota)}b_{k,m}^{(\iota)} + \left(\lambda_m^{(\iota)}I_{N_t} - \Psi_m^{(\iota)}\right)w_k^{(\iota)}(m) \tag{82}$$

Then we have (83). Thus, (81) is decomposed into $N_t$ indpendent subproblems as follows:

$$\begin{aligned} \max_{\mathbf{w}_{k,i}(m)} \sum_{m=0}^{M-1}\sum_{k=1}^{K}\Big[2\Re\{d_{k,i}^*(m)\mathbf{w}_{k,i}(m)\} - \lambda_m^{(\iota)}|\mathbf{w}_{k,i}(m)|^2\Big] \\ \text{s.t.} \quad (1+\frac{L}{M})\sum_{k=1}^{K}\sum_{m=0}^{M-1}|\mathbf{w}_{k,i}(m)|^2 \leq P/N_t, \end{aligned} \tag{84}$$

where the closed-form solution of each subproblem takes the following form:

$$w_{k,i}^{(\iota+1)}(m) = \begin{cases} d_{k,i}(m)/\lambda_m^{(\iota)} \\ \text{if } (1+\frac{L}{M})\sum_{k=1}^{K}\sum_{m=0}^{M-1}\frac{|d_{k,i}(m)|^2}{(\lambda_m^{(\iota)})^2} \leq P/N_t \\ d_{k,i}(m)/(\lambda_m^{(\iota)}+\mu_m) \qquad \text{otherwise} \end{cases} \tag{85}$$

with $\mu_m$ found by bisection, such that

$$(1+\frac{L}{M})\sum_{k=1}^{K}\sum_{m=0}^{M-1}\frac{|d_{k,i}(m)|^2}{(\lambda_m^{(\iota)}+\mu_m)^2} = P/N_t. \tag{86}$$

### B. PREs alternating iteration

It is plausible that the PREs alternating iteration is still based on the closed-form expression (66) .

$$\sum_{k=1}^{K}(\mathbf{w}_k(m))^H\Psi_m^{(\iota)}\mathbf{w}_k(m) = \lambda_m^{(\iota)}\sum_{k=1}^{K}||\mathbf{w}_k(m)||^2-\sum_{k=1}^{K}\mathbf{w}_k^H(m)\left(\lambda_m^{(\iota)}I_{N_t}-\Psi_m^{(\iota)}\right)\mathbf{w}_k(m) \tag{72}$$

$$\leq \lambda_m^{(\iota)}\sum_{k=1}^{K}||\mathbf{w}_k(m)||^2+\sum_{k=1}^{K}(w_k^{(\iota)}(m))^H\left(\lambda_m^{(\iota)}I_{N_t}-\Psi_m^{(\iota)}\right)w_k^{(\iota)}(m) -2\Re\{\sum_{k=1}^{K}(w_k^{(\iota)}(m))^H\left(\lambda_m^{(\iota)}I_{N_t}-\Psi_m^{(\iota)}\right)\mathbf{w}_k(m)\}, \tag{73}$$

for

$$\lambda_m^{(\iota)}\triangleq\lambda_{\max}(\Psi_m^{(\iota)}), m\in\mathcal{M}, \tag{74}$$

---

$$f_{b,m}^{(\iota)}(\mathbf{w}(m)) \geq \tilde{a}_m^{(\iota)}-\lambda_m^{(\iota)}\sum_{k=1}^{K}||\mathbf{w}_k(m)||^2+2\sum_{k=1}^{K}\Re\{\langle\gamma_k^{(\iota)}b_{k,m}^{(\iota)}+\left(\lambda_m^{(\iota)}I_{N_t}-\Psi_m^{(\iota)}\right)w_k^{(\iota)}(m),\mathbf{w}_k(m)\rangle\} \tag{75}$$

$$\triangleq \tilde{f}_{b,m}^{(\iota)}(\mathbf{w}(m)), \tag{76}$$

where

$$\tilde{a}_m^{(\iota)}\triangleq\sum_{k=1}^{K}\gamma_k^{(\iota)}a_{k,m}^{(\iota)}+\sum_{k=1}^{K}(w_k^{(\iota)}(m))^H(\lambda_m^{(\iota)}I_{N_t}-\Psi_m^{(\iota)})w_k^{(\iota)}(m). \tag{77}$$

---

$$\sum_{m=0}^{M-1}f_{b,m}^{(\iota)}(\mathbf{w}(m)) \geq \tilde{a}^{(\iota)}-\sum_{m=0}^{M-1}\lambda_m^{(\iota)}\sum_{k=1}^{K}||\mathbf{w}_k(m)||^2 +2\sum_{m=0}^{M-1}\left(\sum_{k=1}^{K}\Re\{\langle\gamma_k^{(\iota)}b_{k,m}^{(\iota)}+\left(\lambda_m^{(\iota)}I_{N_t}-\Psi_m^{(\iota)}\right)w_k^{(\iota)}(m),\mathbf{w}_k(m)\rangle\}\right) \tag{78}$$

$$\triangleq \tilde{f}_{b,m}^{(\iota)}(\mathbf{w}), \tag{79}$$

where

$$\tilde{a}^{(\iota)}\triangleq\sum_{m=0}^{M-1}\tilde{a}_m^{(\iota)}. \tag{80}$$

---

$$\begin{aligned}\tilde{f}_{b,m}^{(\iota)}(\mathbf{w}) &= \tilde{a}^{(\iota)}-\sum_{m=0}^{M-1}\lambda_m^{(\iota)}\sum_{k=1}^{K}||\mathbf{w}_k(m)||^2+2\sum_{m=0}^{M-1}\left(\sum_{k=1}^{K}\Re\{\langle d_k(m),\mathbf{w}_k(m)\rangle\}\right)\\ &= \tilde{a}^{(\iota)}-\sum_{m=0}^{M-1}\lambda_m^{(\iota)}\sum_{k=1}^{K}||\mathbf{w}_k(m)||^2+2\sum_{m=0}^{M-1}\sum_{k=1}^{K}\sum_{i=1}^{N_t}\Re\{d_{k,i}^*(m)\mathbf{w}_{k,i}(m)\}\\ &= \tilde{a}^{(\iota)}+\sum_{i=1}^{N_t}\left[-\sum_{m=0}^{M-1}\lambda_m^{(\iota)}\sum_{k=1}^{K}|\mathbf{w}_{k,i}(m)|^2+2\left(\sum_{m=0}^{M-1}\sum_{k=1}^{K}\Re\{d_{k,i}^*(m)\mathbf{w}_{k,i}(m)\}\right)\right].\end{aligned} \tag{83}$$

---

### C. Algorithm

The pseudo-code for (85) and (66) is provided by Algorithm 4.

## VI. Numerical examples

In this section, we evaluate the effectiveness of the proposed algorithms. The numerical values of the main simulation parameters are provided by Table II, which are mainly taken from [21], [32]. The Rician factor of the small-scale fading channel gain $H_{\text{B-R}}$ of the BS to RIS and the RIS to UE $k$ gain $h_{\text{R-k}}$ is set to 10 dB. $[\mathcal{R}_{\text{R-k}}]_{n,n'}=e^{j\pi(n-n')\sin\tilde{\phi}_k\sin\tilde{\theta}_k}$ represents the spatial correlation matrix, where the azimuth and elevation angle for UE $k$ are $\tilde{\phi}_k$ and $\tilde{\theta}_k$, respectively. For the channel from BS to RIS, the number of taps is set to $L_1=2$, and for the channel of RIS to UE $k$, the number of taps is set to $L_2=4$ as the distance between the nearby edge user and the RIS is relatively short. The BS is deployed at the coordinates of $(20,0,25)m$, the RIS is positioned at $(0,30,40)m$, and at the right-hand-side of RIS and the obstacles, all UEs are randomly placed in a $30m\times30m$ square area. The following legends are used to identify the

**Algorithm 4** Per-antenna power-constrained GM-rate optimization

1: **Initialization:** Set $\iota = 0$. Generate random $(w^{(0)}, \theta^{(0)})$ meeting the constraint (67) and calculate $\gamma_k^{(0)}$ by (44).
2: **Repeat until convergence of the OF in** (68)**:** calculate $w^{(\iota+1)}$ by (85) and $\theta^{(\iota+1)}$ by (66). Reset $\iota = \iota + 1$.
3: **Output** $(w^{(\iota)}, \theta^{(\iota)})$ and the user rates $\rho_k(w^{(\iota)}, \theta^{(\iota)})$, $k \in \mathcal{K}$.

proposed implementations:

- CVX SR, CVX WR and CVX GM represent the performance of SR, WR and GM-rate optimization based on a universal convex solver assisted Algorithm 1, respectively;
- Closed-form GM and 3-bit closed-form GM denote the $b = \infty$ and $b = 3$ performance of GM-rate optimization based on Algorithm 2, respectively;
- Closed-form SR and 3-bit closed-form SR correspond to the $b = \infty$ and $b = 3$ performance of SR optimization based on Algorithm 3, respectively;
- Per-antenna GM and 3-bit per-antenna GM indicate the $b = \infty$ and $b = 3$ performance of GM-rate optimization based on the per-antenna power-constrained Algorithm 4, respectively.
- Closed-form GM w. random $\theta$ and Per-antenna GM w. random $\theta$ depict the performance of Closed-form GM and Per-antenna GM under random PREs, respectively.

### A. Illustrative validation based on a simple example

Owing to the high computational complexity of the universal convex solver based Algorithm 1, a simple example relying on $(N_t, K, M, N) = (3, 3, 8, 100)$ and $P = 25$ dBm is used for analyzing and comparing the SR and WR achieved by the proposed algorithms.

Figure 2 depicts the typical convergence behavior of the proposed algorithms, with the objective function value normalized using a min-max normalization strategy to facilitate comparison. Upon examination, it is apparent that the CVX SR and CVX GM algorithms demonstrate an accelerated convergence. Remarkably, all of the proposed algorithms are capable of attaining 70% of their respective optimal solutions within a span of 10 iterations.

Figures 3 and 4 plot the sum-rate versus the number of BS antennas $N_t$ and and the number of RIS elements $N$, respectively. We can observe that the achievable sum-rate improves upon increasing $N_t$ or $N$. Similarly, Figures 5 and 6 plot the worst-rate versus $N_t$ and $N$, respectively and we can also witness the improvement in the worst-case user-rate upon increasing $N_t$ or $N$.

Fig. 3 and Fig. 4 plot the SR versus the number of antennas $N_t$ and the number of RIS elements $N$, respectively. Furthermore, Fig. 5 and Fig. 6 demonstrate the WR attained versus $N_t$ and $N$, respectively. Remarkably, we observe an improvement in the both SR and WR upon increasing $N_t$ or $N$. Observe that:

- As expected, CVX SR and Closed-form SR achieve the highest SR, but the lowest (zero) WR. Therefore, SR is a deficient optimization objective for MU OFDM as it offers inadequate services for some users maximizing the SR;
- CVX WR attains the best WR but the worst SR, i.e. WR maximization sacrifices the SR to achieve the highest WR;
- CVX GM and Closed-form GM achieve both competitive SR and WR, i.e. GM-rate maximization achieves Pareto optimality for the multi-objective SR and WR optimization. More importantly, it provides rate-fairness for all users;
- Per-antenna GM achieves a lower SR and WR than Closed form GM, because the per-antenna power constraints (67) is much stricter than the sum-power constraint (23);
- Convex-solver based Algorithm 1 and Closed-form based Algorithm 2 have similar performance, but the complexity of the former is much higher compared to that of the latter.

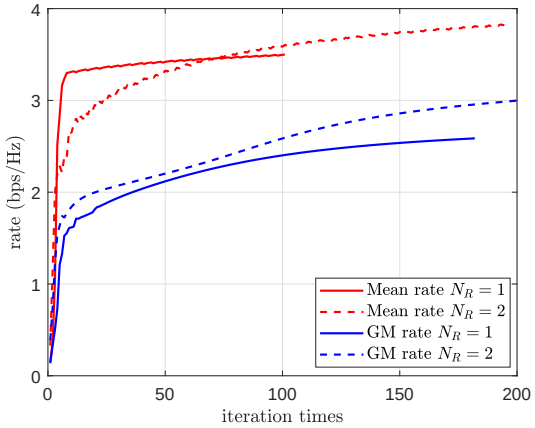


Fig. 2: Convergence for SR, WR and GM algorithms.

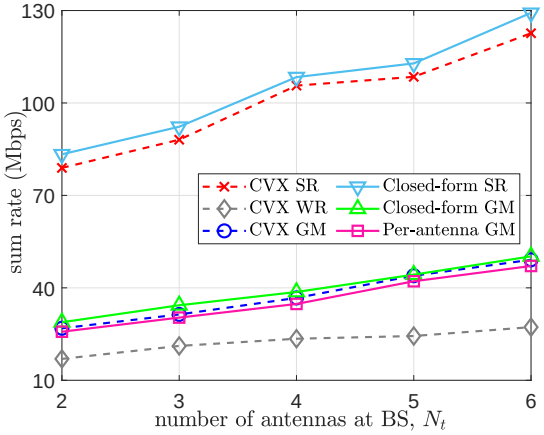


Fig. 3: SR vs. the number of antennas, $N_t$.

### B. Performance Analysis

TABLE II: Main parameters

| Parameter | Numerical value |
|---|---|
| Bandwidth | 100MHz |
| Noise power density | $-174$ dBm/Hz |
| Antenna gain $G_{\text{BS}}$ of the BS | 5 dBi |
| Antenna gain $G_{\text{RIS}}$ of the RIS elements | 5 dBi |
| BS-to-RIS path-loss $\beta_{\text{B-R}}$ under $d_{\text{B-R}}$ | $G_{\text{BS}} + G_{\text{RIS}} - 35.9 - 22\log_{10}(d_{\text{B-R}})$ (in dB) |
| RIS-to-UE path-loss $\beta_{\text{R-k}}$ under $d_{\text{R-k}}$ | $G_{\text{RIS}} - 33.05 - 30\log_{10}(d_{\text{R-k}})$ (in dB) |

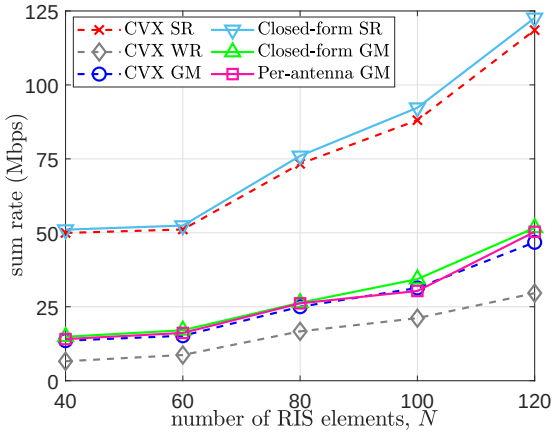


Fig. 4: SR vs. the number of RIS elements, $N$.

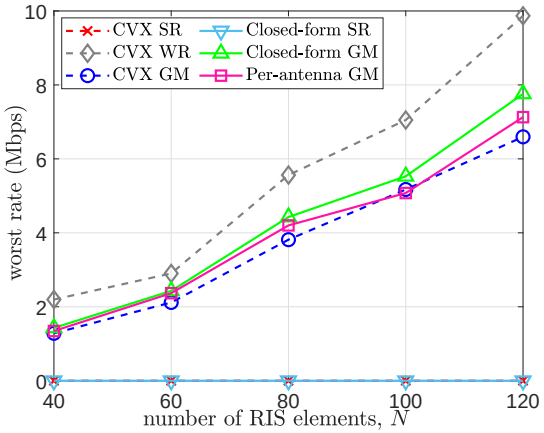


Fig. 6: WR vs. the number of RIS elements, $N$.

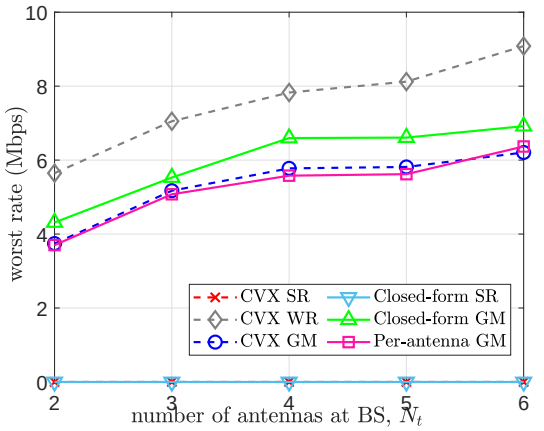


Fig. 5: WR vs. the number of antennas, $N_t$.

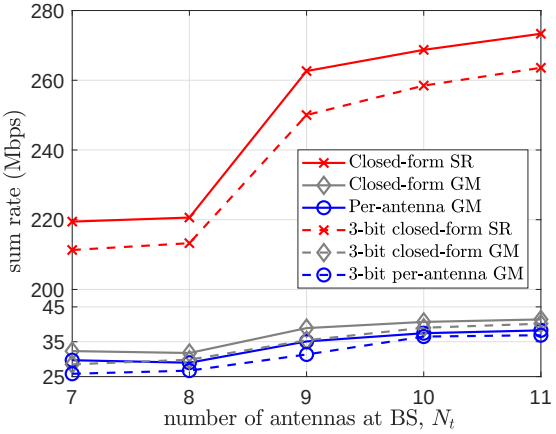


Fig. 7: SR vs. the number of antennas, $N_t$.

Since the convex-solver based Algorithm 1 has high computational complexity, it is unattractive for practical scenarios. Hence from now we shall analyse the performances of the Algorithm 2, 3, and 4, which are closed-form based. Unless stated otherwise, $(N_t, K, M, N) = (10, 10, 64, 100)$ and $P = 35$ dBm are set.

Fig. 7 illustrates the SR performance versus $N_t$ attained by the closed-form based algorithms. Explicitly, Fig. 7 shows that the Closed-form SR has the best performance, Closed-form GM has better performance than Per-antenna GM, and their 3-bit resolution counterparts follow the same trend. As expected, all the proposed infinite PRE-resolution algorithms have better performance than their 3-bit counterparts, and the performance of the algorithms advocated improve upon increasing the number of BS antennas.

Fig. 8 plots the WR achieved by the proposed closed-form based algorithms. Closed-form GM and Per-antenna GM achieve higher WR than Closed-form SR, and their 3-bit resolution counterparts follow the same trend. Furthermore, the WR achieved by Closed-form SR and 3-bit closed-form SR are close to zero, demonstrating that SR based algorithms are incapable of providing adequate rates for all users. Moreover, the WR achieved does get better with the increase of of BS antennas number.

Fig. 9 allows us to examine the rate distribution pattern under $(N_t, N, P) = (10, 100, 35\text{dBm})$. Observe that Closed-form SR and its 3-bit resolution counterparts are incapable of avoiding zero rate be assigned to some users, hence demonstrating the superiority of the GM rate based algorithms.

To validate the fact that the GM-rate based algorithms have a

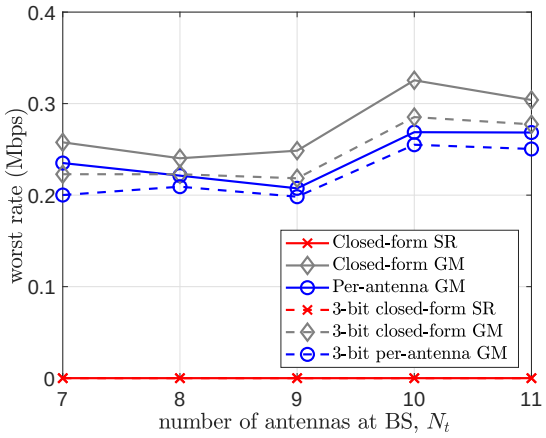


Fig. 8: WR vs. the number of antennas, $N_t$.

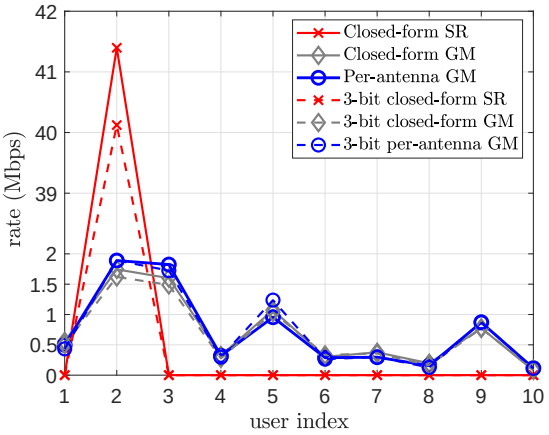


Fig. 9: Rate distribution for $N_t = 10$.

better rate distribution, Table III and Table IV provide the min-rate/max-rate and variance/(mean rate)$^2$ versus the BS antennas number for the proposed algorithms, respectively. Table III shows that Closed-form GM has the best overall performance, and the min-rate/max-rate of SR based algorithms remains zero, which confirms the inability of avoiding zero rate for each UE. Table IV shows that Closed-form GM has the best performance, Closed-form SR has the worst rate distribution, even though its SR is better than Closed-form GM and Per-antenna GM. Their 3-bit resolution counterparts follow the same trend, confirming the advantage of employing GM-rate optimization and the efficiency of the proposed b-bit resolution algorithms.

Furthermore, we utilize Jain's fairness index (JFI) to assess the user fairness as defined by [47]:

$$JFI = \frac{(\sum_{k=1}^{K} \rho_k(\mathbf{w}, \boldsymbol{\theta}))^2}{K \sum_{k=1}^{K} \rho_k(\mathbf{w}, \boldsymbol{\theta})^2}. \quad (87)$$

The users' Jain fairness index for the proposed algorithms is provided in Fig. 10. Observe that the Jain's fairness index for Closed-form GM, Per-antenna GM and their 3-bit resolution counterparts is around 0.45, while for Closed-form SR and for its 3-bit resolution counterpart is around 0.1. Furthermore, it can be observed that Jain's fairness index is not a monotonic function of BS antennas number.

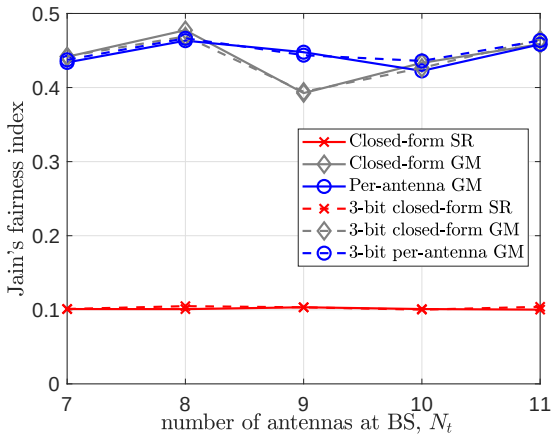


Fig. 10: JFI vs. the number of antennas, $N_t$.

Next, we examine the SR and WR upon varying RIS elements number $N$ in Fig. 11 and Fig. 12, respectively. Fig. 11 shows that Closed-form SR has the best SR, Closed-form GM has a better SR than Per-antenna GM, and the performance of all the proposed algorithms improves with the increas of RIS elements number. In Fig. 12, it can be observed that Closed-form GM has the highest WR, while the WR of Closed-form SR remains zero, and their 3-bit resolution counterparts follow the similar trend. The superiority of Closed-form GM can also be observed in Fig. 13 and Fig. 14, which plot the SR and WR upon varying the transmit power budget $P$ at the BS, respectively. Moreover, the above results also show the efficiency of the proposed 3-bit resolution counterparts.

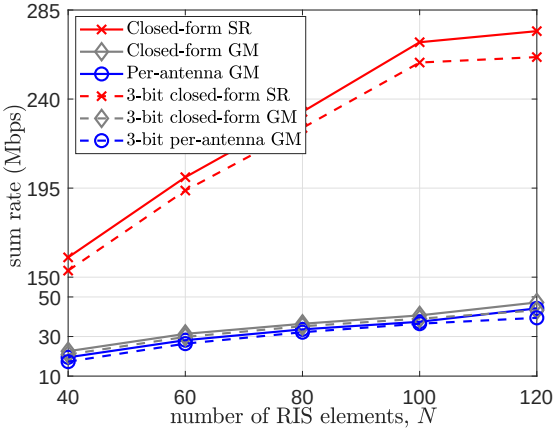


Fig. 11: SR vs. the number of RIS elements, $N$.

Finally, Fig. 15 and Fig. 16 allow us to analyze the SR and WR performance achieved by the $b$-bit resolution algorithms under different values of $b$. Similar to our previous observations, b-bit closed-form SR has the best SR, while b-bit closed-form GM has the highest WR. Fig. 15 and Fig. 16 also provides compelling evidence that the proposed

TABLE III: Min-rate/max-rate ratio vs. the number of antennas at the BS

| Number of antennas | Closed-form SR | Closed-form GM | Per-antenna GM | 3-bit Closed -form SR | 3-bit Closed -form GM | 3-bit per -antenna GM |
|---|---|---|---|---|---|---|
| $N_t = 7$ | 0 | 0.0610 | 0.0543 | 0 | 0.0563 | 0.0476 |
| $N_t = 8$ | 0 | 0.0502 | 0.0469 | 0 | 0.0466 | 0.0478 |
| $N_t = 9$ | 0 | 0.0333 | 0.0309 | 0 | 0.0339 | 0.0318 |
| $N_t = 10$ | 0 | 0.0478 | 0.0387 | 0 | 0.0425 | 0.0440 |
| $N_t = 11$ | 0 | 0.0544 | 0.0519 | 0 | 0.0556 | 0.0525 |

TABLE IV: Variance/(mean rate)$^2$ ratio vs. the number of antennas at the BS

| Number of antennas | Closed-form SR | Closed-form GM | Per-antenna GM | 3-bit Closed -form SR | 3-bit Closed -form GM | 3-bit per -antenna GM |
|---|---|---|---|---|---|---|
| $N_t = 7$ | 8.9187 | 2.0324 | 2.0900 | 8.9123 | 1.9498 | 2.0245 |
| $N_t = 8$ | 8.9296 | 1.7176 | 1.8052 | 8.6725 | 1.7773 | 1.7919 |
| $N_t = 9$ | 8.8278 | 2.3709 | 2.4188 | 8.8334 | 2.3602 | 2.4222 |
| $N_t = 10$ | 8.9999 | 2.0904 | 2.1953 | 8.9775 | 2.1694 | 2.2157 |
| $N_t = 11$ | 8.8164 | 1.8045 | 1.8626 | 8.7687 | 1.7713 | 1.8069 |

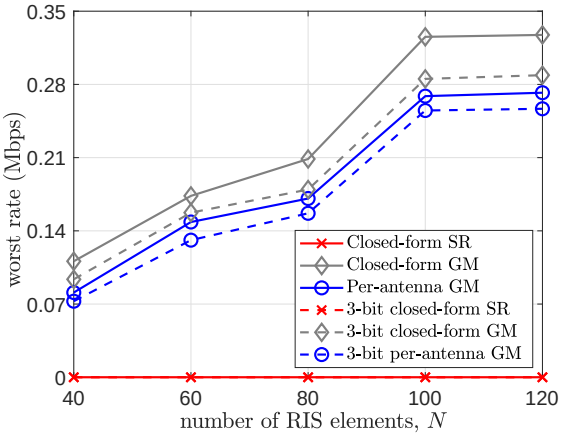


Fig. 12: WR vs. the number of RIS elements, $N$.

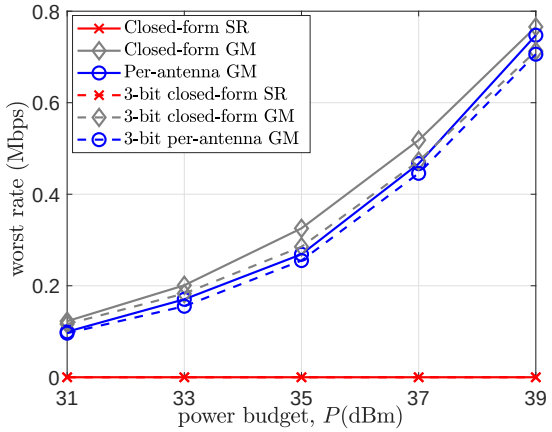


Fig. 14: WR vs. transmit power budget at the BS, $P$.

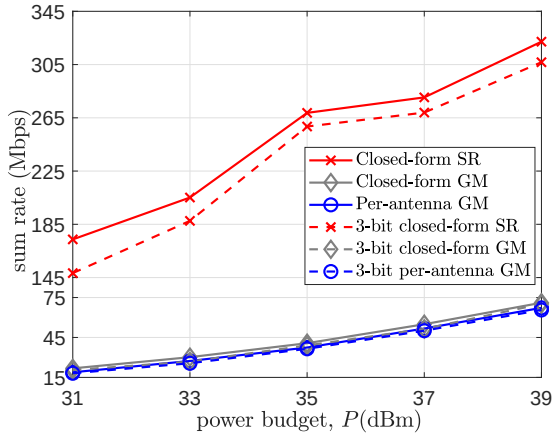


Fig. 13: SR vs. transmit power budget at the BS, $P$.

Closed-form GM and Per-antenna GM algorithms significantly outperform their counterparts, the Closed-form GM w. random $\theta$ and Per-antenna GM w. random $\theta$, respectively. This clearly demonstrates the superiority of our proposed algorithms. Furthermore, the WR of b-bit closed-form SR remains zero, which confirms its inability of avoiding the zero rates for each UE. Moreover, the WR and SR achieved by b-bit closed-form GM and b-bit per-antenna GM for $b \geq 2$ are close to their infinite resolution counterparts, confirming the superiority of the proposed $b$-bit algorithms.

## VII. Summary and Conclusions

The rate-fairness provided by MU OFDM has been an open problem in the literature due its computational intractability. The problem becomes much more computationally challenging for RIS-aided MU OFDM due its large-scale mixed discrete continuous optimization nature. This treatise has opened a new way of addressing the rate-fairness of MU OFDM by developing closed-form based algorithms of scalable complexity for solving the GM-rate optimization problem. Indeed, GM-rate maximization has been shown to attain both a competitive worst rate and sum rate, yielding the multi-objective WR and SR optimization problem arrives at a Pareto optimal solution.

## References

[1] C. Liaskos, S. Nie, A. Tsioliaridou, A. Pitsillides, S. Ioannidis, and I. Akyildiz, "A new wireless communication paradigm through software-

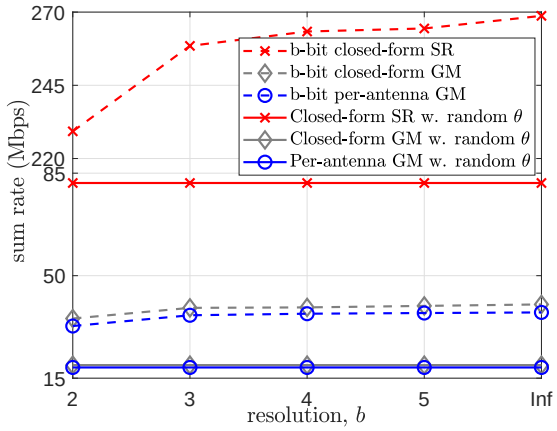


Fig. 15: SR vs. resolution, $b$.

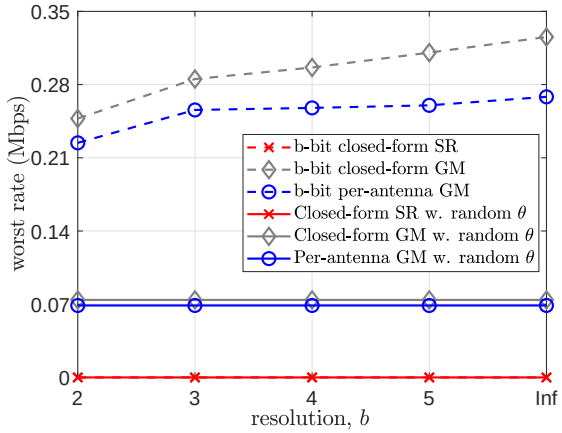


Fig. 16: WR vs. resolution, $b$.

controlled metasurfaces," *IEEE Commun. Mag.*, vol. 56, no. 9, pp. 162–169, 2018.

[2] M. Di Renzo, A. Zappone, M. Debbah, M. S. Alouini, C. Yuen, J. De Rosny and S. A. Tretyakov, "Smart radio environments empowered by reconfigurable intelligent surfaces: How it works, state of research, and the road ahead," *IEEE J. Sel. Areas Commun.*, vol. 38, no. 11, pp. 2450–2525, 2020.

[3] C. Pan, G. Zhou, K. Zhi, S. Hong, T. Wu, Y. Pan, H. Ren, M. Di Renzo, A. L. Swindlehurst, R. Zhang and A. Y. Zhang , "An overview of signal processing techniques for RIS/IRS-aided wireless systems," *IEEE J. Selec. Topics Signal Process.*, vol. 16, pp. 883–917, May 2022.

[4] E. Bjornson, H. Wymeersch, B. Matthiesen, P. Popovski, L. Sanguinetti and E. De Carvalho, "Reconfigurable intelligent surfaces: A signal processing perspective with wireless applications," *IEEE Signal Process. Mag.*, vol. 39, pp. 135–158, Feb. 2022.

[5] C. Pan, H. Ren, K. Wang, W. Xu, M. Elkashlan, A. Nallanathan, and L. Hanzo, "Multicell MIMO communications relying on intelligent reflecting surface," *IEEE Trans Wirel. Commun.*, vol. 19, pp. 5218–5233, Aug. 2020.

[6] C. Pan, H. Ren, K. Wang, M. Elkashlan, A. Nallanathan, J. Wang, and L. Hanzo, "Intelligent reflecting surface aided MIMO broadcasting for simultaneous wireless information and power transfer," *IEEE J. Sel. Areas Commun.*, vol. 38, pp. 1719–1734, Aug. 2020.

[7] Y. Pan, K. Wang, C. Pan, H. Zhu, and J. Wang, "Sum-rate maximization for intelligent reflecting surface assisted terahertz communications," *IEEE Trans. Veh. Tech.*, vol. 71, no. 3, pp. 3320–3325, 2022.

[8] H. Xie, J. Xu, and Y.-F. Liu, "Max-min fairness in IRS-aided multi-cell MISO systems with joint transmit and reflective beamforming," *IEEE Trans. Wirel. Commun.*, vol. 20, pp. 1379–1393, Feb. 2021.

[9] H. Yu, H. D. Tuan, A. A. Nasir, T. Q. Duong, and H. V. Poor, "Joint design of reconfigurable intelligent surfaces and transmit beamforming under proper and improper Gaussian signaling," *IEEE J. Sel. Areas Commun.*, vol. 38, pp. 2589–2603, Nov. 2020.

[10] J. Qiu, J. Yu, A. Dong, and K. Yu, "Joint beamforming for IRS-aided multi-cell MISO system: Sum rate maximization and SINR balancing," *IEEE Trans. Wirel. Commun.*, vol. 21, pp. 7536–7549, Sept. 2022.

[11] H. Yu, H. D. Tuan, E. Dutkiewicz, H. V. Poor, and L. Hanzo, "Maximizing the geometric mean of user-rates to improve rate-fairness: Proper vs. improper Gaussian signaling," *IEEE Trans. Wirel. Commun.*, vol. 21, no. 1, pp. 295–309, 2022.

[12] A. A. Nasir, H. D. Tuan, E. Dutkiewicz, H. V. Poor, and L. Hanzo, "Low-resolution RIS-aided multiuser MIMO signaling," *IEEE Trans. Commun.*, vol. 70, pp. 6517–6531, Oct. 2022.

[13] Y. Yang, S. Zhang, and R. Zhang, "IRS-enhanced OFDMA: Joint resource allocation and passive beamforming optimization," *IEEE Wirel. Commun. Lett.*, vol. 9, no. 6, pp. 760–764, 2020.

[14] W. R. Ghanem, V. Jamali, and R. Schober, "Joint beamforming and phase shift optimization for multicell IRS-aided OFDMA-URLLC systems," in *Proc. IEEE Wirel. Commun. Netw. Conf. (WCNC)*, pp. 1–7, 2021.

[15] Z. Wei, Y. Cai, Z. Sun, D. W. K. Ng, J. Yuan, M. Zhou and L. Sun, "Sum-rate maximization for IRS-assisted UAV OFDMA communication systems," *IEEE Trans. Wirel. Commun.*, vol. 20, pp. 2530–2550, Apr. 2021.

[16] W. Hao, G. Sun, M. Zeng, Z. Chu, Z. Zhu, O. A. Dobre and P. Xiao, "Robust design for intelligent reflecting surface-assisted MIMO-OFDMA Terahertz IoT networks," *IEEE Int. Things J.*, vol. 8, pp. 13052–13064, Aug. 2021.

[17] A. Goldsmith, *Wireless Commununications*. New York, NY, USA: Cambridge University Press, 2005.

[18] Y. Yang, B. Zheng, S. Zhang, and R. Zhang, "Intelligent reflecting surface meets OFDM: Protocol design and rate maximization," *IEEE Trans. Commun.*, vol. 68, pp. 4522–4535, Jul. 2020.

[19] K. Feng, Y. Chen, Y. Han, X. Li, and S. Jin, "Passive beamforming design for reconfigurable intelligent surface-aided OFDM: A fractional programming based approach," in *Proc. IEEE Veh. Techn. Conf. (VTC)*, pp. 1–6, 2021.

[20] Z. He, H. Shen, W. Xu, and C. Zhao, "Low-cost passive beamforming for RIS-aided wideband OFDM systems," *IEEE Wirel. Commun. Lett.*, vol. 11, no. 2, pp. 318–322, 2022.

[21] E. Bjornson, O. Ozdogan, and E. G. Larsson, "Intelligent reflecting surface versus decode-and-forward: How large surfaces are needed to beat relaying?," *IEEE Wirel. Commun. Lett.*, vol. 9, no. 2, pp. 244–248, 2020.

[22] L. Hanzo, B. Choi, T. Keller, *et al.*, *OFDM and MC-CDMA for broadband multi-user communications, WLANs and broadcasting*. John Wiley & Sons, 2005.

[23] W. Yu and R. Lui, "Dual method for nonconvex spectrum optimization of multicarrier systems," *IEEE Trans. Commun.*, vol. 54, pp. 1310–1322, July 2006.

[24] J. Papandriopoulos and J. S. Evans, "SCALE: a low-complexity distributed protocol for spectrum balancing in multi-user DSL networks," *IEEE Trans. Info. Theory*, vol. 55, pp. 3711–3724, Aug. 2009.

[25] A. A. Nasir, H. D. Tuan, E. Dutkiewicz, H. V. Poor, and L. Hanzo, "Relay-aided multi-user OFDM relying on joint wireless power transfer and self-interference recycling," *IEEE Trans. Commun.*, vol. 70, pp. 291–305, Jan 2022.

[26] H. Li, W. Cai, Y. Liu, M. Li, Q. Liu and Q. Wu, "Intelligent reflecting surface enhanced wideband MIMO-OFDM communications: From practical model to reflection optimization," *IEEE Trans. Commun.*, vol. 69, pp. 4807–4820, Jul. 2021.

[27] B. Di, H. Zhang, L. Li, L. Song, Y. Li, and Z. Han, "Practical hybrid beamforming with finite-resolution phase shifters for reconfigurable intelligent surface based multi-user communications," *IEEE Trans. Veh. Tech.*, vol. 69, no. 4, pp. 4565–4570, 2020.

[28] H. Zhang, B. Di, L. Song, and Z. Han, "Reconfigurable intelligent surfaces assisted communications with limited phase shifts: How many phase shifts are enough?," *IEEE Trans. Veh. Tech.*, vol. 69, no. 4, pp. 4498–4502, 2020.

[29] H. H. M. Tam, H. D. Tuan, and D. T. Ngo, "Successive convex quadratic programming for quality-of-service management in full-duplex MU-MIMO multicell networks," *IEEE Trans. Commun.*, vol. 64, pp. 2340–2353, June 2016.

[30] H. Tuy, *Convex Analysis and Global Optimization (second edition)*. Springer International, 2017.

[31] T. Van Chien, H. Q. Ngo, S. Chatzinotas, M. Di Renzo, and B. Ottersten, "Reconfigurable intelligent surface-assisted cell-free massive

MIMO systems over spatially-correlated channels," *IEEE Trans. Wirel. Commun.*, vol. 21, no. 7, pp. 5106–5128, 2022.

[32] Q. U. A. Nadeem, A. Kammoun, A. Chaaban, M. Debbah, and M. S. Alouini, "Asymptotic max-min SINR analysis of reconfigurable intelligent surface assisted MISO systems," *IEEE Trans. Wirel. Commun.*, vol. 19, no. 12, pp. 7748–7764, 2020.

[33] Q.-U.-A. Nadeem, A. Kammoun, M. Debbah, and M.-S. Alouini, "A generalized spatial correlation model for 3D MIMO channels based on the Fourier coefficients of power spectrums," *IEEE Trans. Signal Process.*, vol. 63, pp. 3671–3686, Jul. 2015.

[34] G. T. de Araujo, A. L. F. de Almeida, and R. Boyer, "Channel estimation for intelligent reflecting surface assisted MIMO systems: A tensor modeling approach," *IEEE J. Selec. Topics Signal Process.*, vol. 15, pp. 789–802, Mar. 2021.

[35] B. Zheng, C. You, W. Mei, and R. Zhang, "A survey on channel estimation and practical passive beamforming design for intelligent reflecting surface aided wireless communications," *IEEE Commun. Surv. Tut.*, vol. 24, no. 2, pp. 1035–1071, 2022.

[36] J. An, C. Xu, L. Wang, Y. Liu, L. Gan, and L. Hanzo, "Joint training of the superimposed direct and reflected links in reconfigurable intelligent surface assisted multiuser communications," *IEEE Trans. Green Commun. Network.*, vol. 6, no. 2, pp. 739–754, 2022.

[37] J. An, C. Xu, L. Gan, and L. Hanzo, "Low-complexity channel estimation and passive beamforming for RIS-assisted MIMO systems relying on discrete phase shifts," *IEEE Trans. Commun.*, vol. 70, pp. 1245–1260, Feb. 2022.

[38] Y. Wei, M.-M. Zhao, M.-J. Zhao, and Y. Cai, "Channel estimation for IRS-aided multiuser communications with reduced error propagation," *IEEE Trans. Wirel. Commun.*, vol. 21, pp. 2725–2741, Apr. 2022.

[39] H. Dong, C. Ji, L. Zhou, J. Dai, and Z. Ye, "Sparse channel estimation with surface clustering for IRS-assisted OFDM systems," *IEEE Trans. Commun.*, vol. 71, no. 2, pp. 1083–1095, 2023.

[40] Y. Lin, S. Jin, M. Matthaiou, and X. You, "Channel estimation and user localization for IRS-assisted MIMO-OFDM systems," *IEEE Trans. Wirel. Commun.*, vol. 21, no. 4, pp. 2320–2335, 2022.

[41] L. Wei, C. Huang, G. C. Alexandropoulos, C. Yuen, Z. Zhang, and M. Debbah, "Channel estimation for RIS-empowered multi-user MISO wireless communications," *IEEE Trans. Commun.*, vol. 69, no. 6, pp. 4144–4157, 2021.

[42] J. He, H. Wymeersch, and M. Juntti, "Channel estimation for RIS-aided mmWave MIMO systems via atomic norm minimization," *IEEE Trans. Wirel. Commun.*, vol. 20, no. 9, pp. 5786–5797, 2021.

[43] H. Liu, X. Yuan, and Y.-J. A. Zhang, "Matrix-calibration-based cascaded channel estimation for reconfigurable intelligent surface assisted multiuser MIMO," *IEEE J. Select. Areas Commun.*, vol. 38, no. 11, pp. 2621–2636, 2020.

[44] Z. Zhou, N. Ge, Z. Wang, and L. Hanzo, "Joint transmit precoding and reconfigurable intelligent surface phase adjustment: A decomposition-aided channel estimation approach," *IEEE Trans. Commun.*, vol. 69, no. 2, pp. 1228–1243, 2021.

[45] W. Zhu, H. D. Tuan, E. Dutkiewicz, Y. Fang, and L. Hanzo, "Low-complexity Pareto-optimal 3D beamforming for the full-dimensional multi-user massive MIMO downlink," *IEEE Trans. Veh. Tech. (early access)*.

[46] A. Migdalas, "A regularization of the Frank-and-Wolfe method and unification of certain nonlinear programming methods," *Math. Program.*, vol. 65, pp. 331–346, 1994.

[47] Y.-K. Hua, W. Chang, and S.-L. Su, "Cooperative scheduling for pilot reuse in massive MIMO systems," *IEEE Trans. Veh. Tech.*, vol. 69, no. 11, pp. 12857–12869, 2020.